



Tandem Mass Tag Labeling–Based Analysis to Characterize Muscle-Specific Proteome Changes During Postmortem Aging of Bison *Longissimus Lumborum* and *Psoas Major* Muscles

Md Mahmudul Hasan¹, Mahamud-ur Rashid², Surendranath P. Suman³, Helene Perreault⁴, Jitendra Paliwal⁵, and Argenis Rodas-Gonzalez^{6,*}

¹Department of Food and Human Nutritional Sciences, University of Manitoba, Winnipeg, MB R3T 2N2, Canada

²Department of Medical Microbiology and Infectious Diseases, University of Manitoba, Winnipeg, MB R3E 0J9, Canada

³Department of Animal and Food Sciences, University of Kentucky, Lexington, KY 40546-0215, USA

⁴Department of Chemistry, University of Manitoba, Winnipeg, MB R3T 2N2, Canada

⁵Department of Biosystems Engineering, University of Manitoba, Winnipeg, MB R3T 2N2, Canada

⁶Department of Animal Science, University of Manitoba, Winnipeg, MB R3T 2N2, Canada

*Corresponding author. Email: Argenis.RodasGonzalez@umanitoba.ca (Argenis Rodas-Gonzalez)

Abstract: The objective of the study was to examine the variations in sarcoplasmic proteomes of bison *longissimus lumborum* (LL) and *psoas major* (PM) muscles during postmortem aging utilizing tandem mass tag isobaric labeling coupled with liquid chromatography–mass spectrometry for the categorization of muscles with muscle-specific inherent color stability. A total of 576 proteins were identified in both bison LL and PM muscles, where 97 proteins were identified as differentially abundant (fold change > 1.5, $P < 0.05$) from the 3 comparisons between muscles during postmortem aging periods (PM vs. LL at 2 d, 7 d, and 14 d). Between muscles, the most abundant protein groups were based on functions such as electron transport chain or oxidative phosphorylation, tricarboxylic acid cycle, adenosine triphosphate transport, carbohydrate metabolism, fatty acid oxidation, chaperones, oxygen transport, muscle contraction, calcium signaling, and protein synthesis. In PM, most of the proteins from electron transport chain, tricarboxylic acid cycle, fatty acid oxidation, adenosine triphosphate and oxygen transport, and muscle contraction were more abundant or exhibited increased expression during aging compared with LL. On the other hand, the proteins involved in carbohydrate metabolism, chaperone function, and protein synthesis mostly exhibited decreased expression in PM muscles relative to LL. These results clearly demonstrate that the proteins associated with oxidative metabolism showed increased expression in PM muscles. This indicates that oxidative damage and subsequent color deterioration resulted in bison PM muscles being attacked by the reactive oxygen species produced during those metabolic processes. In contrast, proteins involved in glycolysis and chaperone activity exhibited a decrease in expression in bison PM muscles, resulting in a decline in color stability compared with LL. Because glycolytic enzymes generate reducing equivalents and chaperones maintain the native folded protein structure, they are consequently responsible for the color stability in LL muscles compared with PM.

Key words: color stability, proteomics, sarcoplasmic proteins, isobaric tags, liquid chromatography–mass spectrometry

Meat and Muscle Biology 6(1): 13055, 1–23 (2021)

doi:10.22175/mmb.13055

Submitted 15 October 2021

Accepted 31 December 2021

Introduction

Fresh meat color is one of the most important characteristics to influence purchase intention (Mancini and Hunt, 2005; Suman et al., 2014). Generally,

consumers are more likely to buy bright cherry-red color meat because it represents meat's freshness and wholesomeness. However, bison meat exhibits a darker appearance, and its color deterioration rate is rapid in aerobically packaged conditions compared

with beef; therefore, color stability has been marked as a critical drawback for the growth of bison meat marketing (Pietrasik et al., 2006; Narváez-Bravo et al., 2017). Moreover, during aging and retail display periods, meat color deterioration leads to product rejection and economic loss (Smith et al., 2000; Canto et al., 2015; Nair et al., 2018).

The rapid discoloration of bison meat could not be attributed to a difference in the biochemistry of bison myoglobin (Mb) per se (identical amino acid sequences and similar oxidation kinetics and thermostability) (Joseph et al., 2010). However, bison have been shown to have a difference in muscle fibre type (Koch et al., 1995; Aalhus et al., 2009), resulting in higher pigment concentration (Galbraith et al., 2016) and higher levels of iron (Marchello and Driskell, 2001; Galbraith et al., 2006) compared with those typically found in beef. In addition, polyunsaturated fatty acid levels (weight percentage) in range-fed and feedlot-fed bison were found to be higher than in range- or feedlot-fed cattle (Rule et al., 2002). Also, malondialdehyde (MDA) critically influences color deterioration patterns in bison muscles and not 4-hydroxy-2-nonenal (HNE) (Hasan et al., 2021), which is contrary to what is observed in beef (Alderton et al., 2003; Suman et al., 2006). Those elements can accelerate Mb oxidation and subsequent meat discoloration. In beef, cellular biochemical mechanisms that govern the color change during postmortem aging affect the muscle-specific sarcoplasmic proteomes (Matarneh et al., 2017; Nair et al., 2018; Xiong, 2018). Furthermore, variations in the balance between antioxidant and pro-oxidant proteins within the sarcoplasm can cause lipid oxidation, lead to Mb oxidation, and cause discoloration in meat (Ramanathan et al., 2009; Joseph et al., 2010). Thus, we hypothesized that the protein profile in bison could differ from beef and explain its inherent rapid color deterioration.

The sarcoplasmic proteins found in beef muscles have been investigated using gel-based proteomic analyses focusing on two-dimensional (2D) gel electrophoresis with label-free approach (Joseph et al., 2012; Suman et al., 2014; Canto et al., 2015; Nair et al., 2018; Yu et al., 2018; Salim et al., 2020). In meat science studies, tandem mass tag (TMT) proteomics is a very recent gel-free approach that has been used for exploring postmortem biochemical and cellular processes in bovine (Zhai et al., 2020), ovine (Li et al., 2018), and porcine (Liu et al., 2018) muscles. The TMT allows a high-throughput approach for the accurate quantification and identification of cellular macromolecules, which help establish interactions and cellular pathways for complex proteomic analysis (Churchman et al.,

2015; Mertz et al., 2015; Wang et al., 2016). Therefore, this study's objective was to examine the changes in sarcoplasmic proteomes in bison *longissimus lumborum* (LL) and *psoas major* (PM) muscles during postmortem aging periods by using TMT labeling coupled with liquid chromatography–mass spectrometry (LC-MS/MS) for the segregation of muscles based on muscle-specific inherent color stability. The study was conducted on muscles supplied by the studies reported by Hasan et al. (2021).

Materials and Methods

Sample collection and processing

This experiment was conducted using bison meat samples as described by Hasan et al. (2021). Briefly, 10 LL (striploin) and 10 PM (tenderloin) muscles from bison A1 grade (<50% ossification on the 9th to 11th thoracic vertebrae cartilaginous caps) (Canada Gazette, 1992) carcasses were purchased from a government-inspected slaughter plant (True North Foods, Carman, MB, Canada) within 48 h postmortem and were transported to the University of Manitoba Food Science Pilot plant (Winnipeg, MB, Canada). Immediately after arrival, muscles were trimmed practically free of subcutaneous fat. From each muscle, a 10 cm-thick section was removed to evaluate biochemistry parameters baseline (Hasan et al., 2021), and then 15 to 20 g of samples were obtained and instantly vacuum packaged (very low-oxygen permeable; FlairPak Vacuum Pouch, Flair Flexible Packaging Corporation, Canada/US) using Vac Master (VAC545, Overland Park, KS) with high vacuum and stored at -80°C for the analysis of sarcoplasmic proteomes. The remaining muscle samples were cut into 2 equal portions, vacuum packed individually, and assigned for an aging period of 7 and 14 d at 2°C . At the end of each assigned aging period, steaks (2.5 cm thick) were obtained for color and biochemistry evaluations, and 15 to 20 g of muscle samples from each muscle portion were collected and stored as described earlier. Samples for color, biochemistry, and proteomic evaluation were obtained randomly starting from the anterior end of the cut alternating anatomical position. Details about the methods applied to evaluate color and biochemical parameters were described by Hasan et al. (2021).

Extraction of sarcoplasmic proteins

Subsamples from 6 LL ($n = 6$) and 6 PM ($n = 6$) frozen (-80°C) muscles from each aging group

(2, 7, and 14 d) were used (total 36 samples; LL01-2D to LL06-2D, LL01-7D to LL06-7D, LL01-14D to LL06-14D, PM01-2D to PM06-2D, PM01-7D to PM06-7D, and PM01-14D to PM06-14D) for the extraction and isolation of sarcoplasmic proteomes. The extraction and other necessary procedures were optimized in the laboratory of the Manitoba Centre for Proteomics and Systems Biology (Winnipeg, MB, Canada). Briefly, 50–60 mg of iced-thawed muscle tissue sample devoid of any subcutaneous fat and connective tissue was cut using 70% ethanol–cleaned blades and weighed on an electronic balance. Each sample was homogenized 4 times in 500 μ L of lysis buffer solution (50 mM HEPES, 5 mM ethylenediaminetetraacetic acid [pH 7.5]; 150 mM NaCl, 1% Triton X100, 1X Protease inhibitor) for 20 s/cycle with a 60-s cooling period on ice each time by using a tissue homogenizer (THP115, 115 V, 144 W, 5,000 to 35,000 rpm; OMNI International Inc., Kennesaw, GA). The homogenate was then centrifuged at 13,000 $\times g$ for 10 min at 4°C (SORVALL LEGEND Micro 21R centrifuge, Thermo Fisher Scientific, Kalkberg, Germany); the supernatant was transferred to another microcentrifuge tube, and the final volume obtained was recorded. The supernatant was kept in ice for 5 min and then stored at –80°C for subsequent analysis. The protein concentration of the sarcoplasmic proteome extract from each sample was determined in duplicate by the Bradford assay (Bradford, 1976) using a protein assay kit (Thermo Fisher Scientific US, Rockford, IL).

Preparation, purification, and digestion of protein samples

The preprocessing of protein samples was performed in 3 steps, namely reduction, alkylation, and quenching. Firstly, for reduction, a 200 μ L aliquot from protein stock was taken in a microcentrifuge tube, and 20 μ L of 20% sodium dodecyl sulphate (SDS) was added to each tube to increase the solubility, reaching a final 2% SDS concentration. Then, 20 μ L of 100 mM dithiothreitol (DTT) was added to the tubes (final concentration of DTT 10 mM), and after vortex mixing, the sample tubes were incubated at 57°C for 30 min. Secondly, after cooling down the reduced incubated sample, alkylation was done by adding 20 μ L of 500 mM iodoacetamide (IAA) to get a final IAA concentration of 50 mM. After mixing well, the sample tubes were placed in a dark place at room temperature for 45 min. Lastly, quenching was done to minimize the excess IAA in the sample mixture by adding 34 μ L of

100 mM DTT to each tube, and then all sample tubes were vortexed for 10 min.

For purification and digestion, 21.1 μ L of sample (containing 100 μ g protein) was pipetted in each microcentrifuge tube, and 10 μ L SP3 beads (from 20 μ g/ μ L preparation) were added. To adjust the pH at 7.0, 21.1 μ L of 200 mM HEPES was added. After adding 121.9 μ L of acetonitrile (70% of final concentration) to each tube, incubated samples were placed in an agitator at room temperature for 18 min and checked for clumping. Then, the sample tubes were put on a magnetic stand, and the supernatant was removed. The SP3 beads were then washed twice with 70% ethanol and one time with 100% acetonitrile. Trypsin was first dissolved in 250 μ L of 50 mM digestion buffer (HEPES at pH 8.0), and 50 μ L of trypsin solution was added to each tube to maintain a final protein concentration of 2 μ g/ μ L. Samples were then sonicated for 20 s to disperse the beads and incubated for 16 h at 37°C. After removing the sample tubes from the incubator, samples were sonicated for 20 s and put on the magnetic stand after spinning the tubes quickly, and the supernatant was transferred to another microcentrifuge tube. Finally, the SP3 beads were washed with 50 μ L of digestion buffer, sample tubes were sonicated again for 20 s and put on the magnetic stand prior to quick spin, and the supernatant was transferred to the previously collected peptide sample tubes. The samples were then stored at –80°C for further analysis.

Tandem mass tag peptide labelling

Prior to peptide labelling by TMT10Plex isobaric label (Thermo Scientific, Rockford, IL; Coleman et al., 2020), peptides from digested protein samples were measured using a quantitative fluorometric peptide assay kit according to the manufacturer's (Thermo Scientific, Rockford, IL) procedure. TMT label reagents were first equilibrated at room temperature. For each vial containing 0.80 mg of label, 41 μ L of anhydrous acetonitrile was added to each tube, the reagent was dissolved by vortexing for 5 min, and the tube was centrifuged briefly to solubilize the label. At first, 41 μ L of the prepared TMT label reagent was added to 100 μ L of sample (containing 25 to 100 μ g protein digest) in a microcentrifuge tube, and the labelling reaction was incubated for 60 min at room temperature. Then, 8 μ L of 5% hydroxylamine was added to the sample followed by incubation for 15 min to quench the reaction. After that, equal amounts of each sample were combined in another microcentrifuge tube, which was subjected to Speedvac vacuum

concentration (Thermo Fisher Scientific US) for drying. Finally, samples were cleaned up on peptide desalting spin columns (Thermo Fisher Scientific US). Additionally, a reference TMT-peptide pool was prepared for TMT LC-MS/MS analysis. The pool was prepared by combining equal volumes of samples LL01-2D, LL01-7D, and LL-01-14D and treated in a similar fashion as the individual samples. An aliquot of the pool was added to every set of TMT sample to account for any instrumental variations across the LC-MS/MS runs.

Liquid chromatography–mass spectrometry analysis

The analysis of TMT labeled protein digests (peptides) was carried out on an Orbitrap Exploris 480 instrument (Thermo Fisher Scientific, Bremen, Germany). Samples were introduced using an Easy-nLC 1000 system (Thermo Fisher Scientific) at 2 μg per injection. Mobile phase A was 0.1% (v/v) formic acid, and mobile phase B was 0.1% (v/v) formic acid in 80% acetonitrile (LC-MS grade). Gradient separation of peptides was performed on a C18 (Luna C18(2), 3- μm particle size; Phenomenex, Torrance, CA) column packed in-house in Pico-Frit (100 μm \times 30 cm) capillaries (New Objective, Woburn, MA). Peptide separation was done using the following gradients: 3% to 7% increase of phase B over 5 min, 7% to 28% over 204 min, 28% to 48% over 15 min, 48% to 95% over 1 min, with final elution of 95% phase B for 15 min at a flow rate of 300 nL/min.

Data acquisition redundant was configured for data-dependent (DD) analysis using the full MS/DD-MS/MS setup in positive mode. The spray voltage was set to 2.3 kV, funnel radio frequency level at 40, and heated capillary at 275°C. Survey scans covering the mass range of 375 to 1,575 m/z were acquired at a resolution of 120,000 (at m/z 200), with a maximum ion injection time of 50 ms and a normalized automatic gain control (AGC) target of 300%. For MS2 scan triggering, up to 20 of the most abundant ions were selected for fragmentation at 36% normalized collision energy, with intensity threshold kept at 2×10^4 . A normalized AGC target value for fragment spectra was set at 200%, and these were acquired at a resolution of 45,000, with a maximum ion injection time of 100 ms and an isolation width set at 0.7 m/z. Dynamic exclusion of previously selected masses was enabled for 45 s, charge state filtering was limited to 2–6, peptide match was set to preferred, and isotope exclusion was on.

MS/MS protein identification and data processing

Each LC-MS/MS run was searched for tryptic peptides against the bison protein database using X! Tandem software (cyclone 2012.10.01.1) with standard Orbitrap settings: 20 ppm each for parent and fragment ions (Coleman et al., 2020). The peptide TMT intensities were integrated over a window of ± 3 mDa and corrected for isotopic overlap using the batch-specific matrix supplied with the TMT label kit. Labels were assigned sequentially as TMT0 to TMT9. Standard variable post-translational modification including oxidation, phosphorylation, cyclization, and deamidation were permitted. Overall, identification efficiency was highly stable: $\sim 30,000$ peptides from $\sim 104,000$ spectra per run. Protein level quantitation required at least 2 unique peptides with expectation values of $\log(e) \leq -1.5$ each, yielding highly confident protein assignments of $\log(e) \leq -3$. $\log(e)$ can be defined as the estimation of likelihood based on the expected number of random matches among 2 peptides. Peptide to protein assignment was handled by X! Tandem. The intensity of each protein for each TMT channel was computed as the sum of the intensities of the member peptides, then converted into \log_2 for differential analysis. These \log_2 expression matrices were normalized (mean = 0, standard deviation = 1) for simplified differential analysis. Total matrix assembly relied on a common pool sample occupying the last TMT channel in every run. On a protein-by-protein basis, the 9 TMT individual sample channels were corrected by subtracting out the reference pool value encoded in the last TMT channel.

Statistical analysis

Data were analyzed by using the Perl 6 programming language (Perl Inc.). The standard deviation pre-normalization for all runs and channels was 2.38; this was used as a scaling factor between (corrected) normalized values back up to the \log_2 scale. These values were also all offset by a constant of 21.35, the pre-normalization average for all runs and channels. Then the pairwise *t* test was conducted, using 6 ($n = 6$) replicates, to investigate the comparisons between different aging periods (time points) and muscle types (LL and PM). Multiple testing corrections were not applied to *P* scores, and any difference with a *P* value of < 0.05 was considered a possibility for biological expedition. The proteins were considered as significantly more or less abundant with the fold change value of > 1.5 and $P < 0.05$.

Bioinformatics analysis

To investigate the overall expression pattern of differentially abundant proteins in LL and PM muscles at different aging times, a heatmap was generated by Morpheus (<https://software.broadinstitute.org/morpheus/>), and the output is presented in Figure 1. Additionally, the distribution of differential proteins (Figure 2) was prepared with the aid of another online tool called InteractiVenn (<http://www.interactivenn.net>; Heberle et al. 2015). Then, the protein–protein interaction networks between identified proteins (Figure 3) were examined using String version 11 (<https://string-db.org/>; Szklarczyk et al., 2019) with the inflation parameter of 3.4 in Markov clustering (Zhai et al., 2020). The proteins are presented as network nodes, and the predicted functional interactions are represented as edges. The proteins were mainly grouped according to their function as stated in the KEGG Pathway database (<https://www.genome.jp/>

kegg/pathway.html) and the Reactome Pathway database (<https://reactome.org>; Fabregat et al., 2018), and a literature search was done to investigate the proteins with limited function. The functional clusters of identified proteins were generated with results obtained from the Panther database (<http://pantherdb.org/>) and are presented in Figure 4. Finally, the Ingenuity pathway analysis (IPA; Qiagen, Redwood City, CA) was performed to examine the most important pathway involved (Figure 5) and the most important protein–protein interaction networks (Figure 6).

Results

Color and biochemical characteristics

Details about color and biochemical parameter results were described by Hasan et al. (2021).

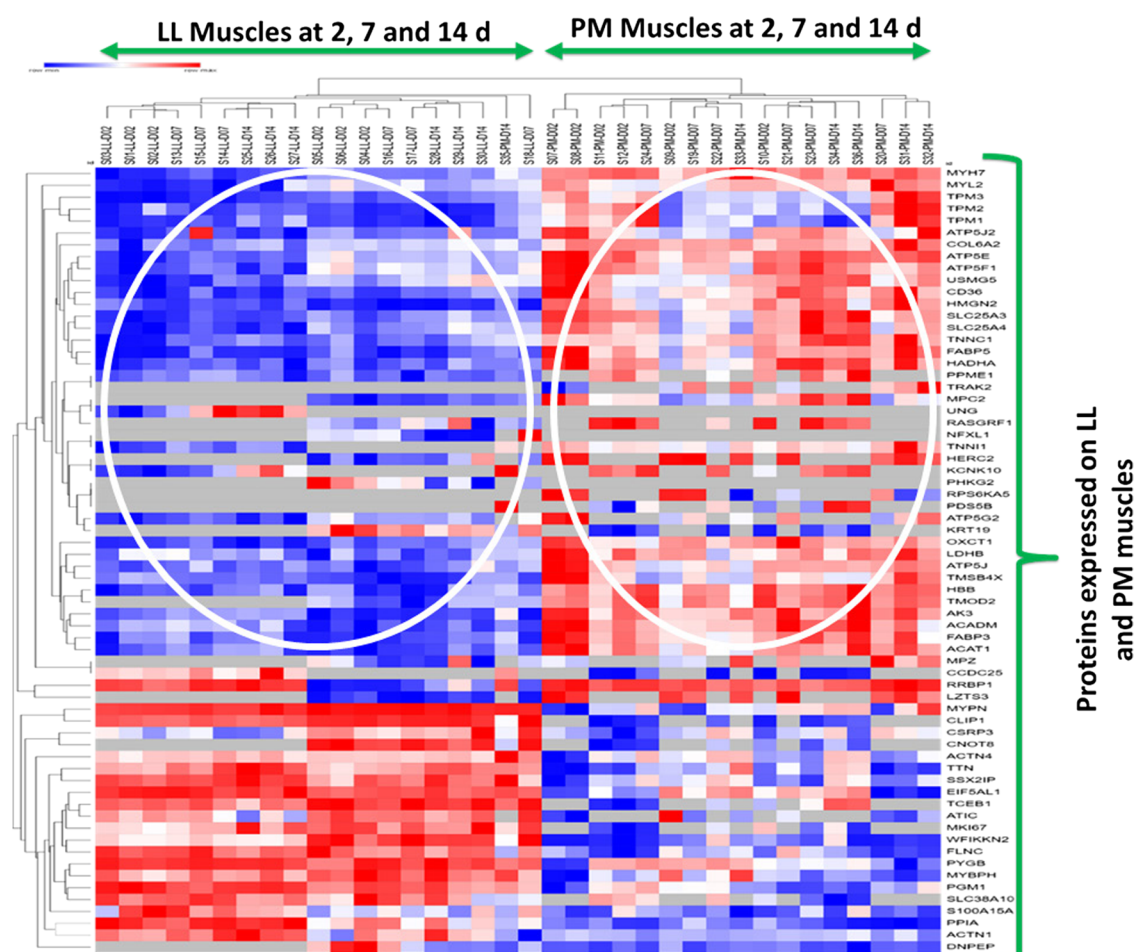


Figure 1. Heatmap showing overall expression of differential proteins ($P < 0.05$, > 1.5 -fold change) in bison *longissimus lumborum* and *psoas major* muscles from different aging periods. (The left and right circles indicates the expression patterns of different proteins at 2, 7 and 14 d postmortem in LL and PM muscles, respectively.); LL = *longissimus lumborum*; PM = *psoas major*; 2, 7 and 14 d = 2 day, 7 day and 14 day postmortem; **Blue color**: decreased expression of proteins; **Red color**: increased expression of proteins

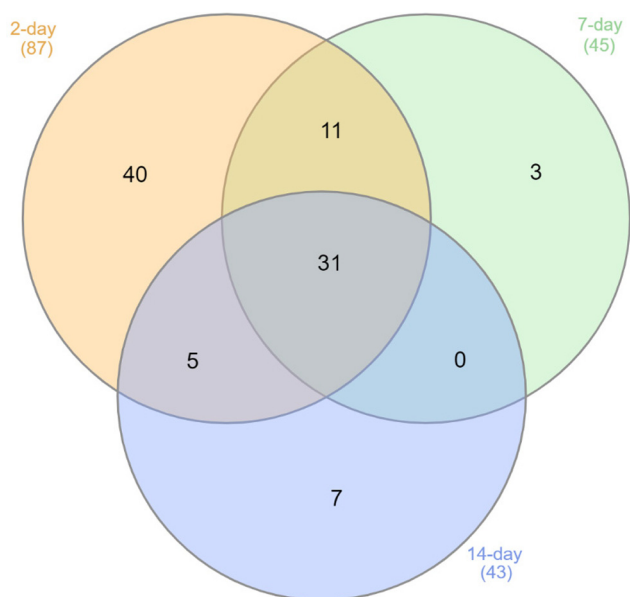


Figure 2. Distribution of differentially abundant proteins between bison *longissimus lumborum* and *psoas major* muscles at 2-d, 7-d and 14-d postmortem aging.

Briefly, Mb (LL = 6.95 vs. PM = 8.12 mg/g) and fat content (LL = 1.55 vs. PM = 2.27%) were included as a covariate in the model owing to difference among muscles ($P < 0.05$). LL showed greater color stability (higher a^* value and lower surface discoloration; $P < 0.05$) than PM and presented lower MDA, HNE, and carbonyl content compared with PM ($P < 0.05$). The pH was not affected by muscle type, retail display, or interactions ($P > 0.05$); only steaks aged for 14 d (5.65) exhibited lower pH values than steaks aged for 7 d (5.79). In both muscles, MDA showed the highest correlation to a^* ($r = -0.78$; $P < 0.01$) and discoloration ($rs = 0.82$; $P < 0.01$) scores, and MDA was the main contributor to redness changes in both muscles, resulting in more remarkable changes in PM ($R^2 > 0.72$) than LL ($R^2 > 0.62$). The pH, HNE, and carbonyl content only explained up to a maximum of 6% of the variation of those attributes in LL steaks, while 1% of the variation in PM color was attributed to those biochemical factors. On the other hand, the principal component analysis indicated that PM and LL steaks aged for 7 and 14 d at day 0 of retail display were closely associated with redness and located far away from oxidation compounds, indicating more red color stability and less oxidation; however, PM steaks aged for 7 and 14 d at day 4 of retail display segregated away from LL, and PM was closely related to oxidation compounds and located far away from redness (representing high oxidation level and less red color).

Comparison of proteomic profiles between LL and PM muscles at each postmortem aging period

A total of 576 proteins were identified by TMT-based proteomic analysis in both LL and PM muscles, and among those, 97 proteins were found to be differentially abundant (fold change > 1.5 , $P < 0.05$) from the 3 comparisons between muscles during postmortem storage periods (PM vs. LL at 2 d, 7 d, and 14 d; Table 1). Among these proteins, the major protein groups identified in muscles (PM vs. LL) are related to electron transport chain (ETC), tricarboxylic acid (TCA) cycle, adenosine triphosphate (ATP) production and transport, carbohydrate metabolism, lipid or fatty acid oxidation, chaperones, oxygen transport, calcium signaling, muscle contraction, and protein synthesis.

In Figure 1, the heatmap presents the overall expression of all differentially abundant proteins in LL and PM muscles from 3 different aging periods. By careful investigation of the heatmap, protein expression changing patterns are quite visible from LL to PM muscles, from LL-D2 to LL-D7, and from PM-D2 to PM-D7 samples. The blue and red colors indicate decreased and increased protein expression levels, respectively (Figure 1). The Venn diagram (Figure 2) represents the overall distribution of 97 differentially abundant proteins identified in LL and PM muscles from 2-, 7-, and 14-d aging periods, and 31 differential proteins were found regardless of postmortem aging times. Most of the differential proteins were identified at 2 d postmortem (87 proteins), whereas 7 d (45 proteins) and 14 d (43 proteins) exhibited almost similar number of proteins between them. This indicates that changes in protein expression occur mainly at the early postmortem stage (2 d) compared with the later periods (7 d and 14 d). Figure 3 exhibits the protein–protein interactions patterns among the differentially abundant proteins identified at 2, 7, and 14 d postmortem. In Figure 3a, 3 visible clusters of proteins were found with proteins involved in ETC, fatty acid oxidation, and muscle contraction at 2 d postmortem. The only protein–protein interaction cluster at 7 d postmortem (Figure 3b) included muscle contraction proteins, whereas Figure 3c shows a slightly different clustering pattern that includes carbohydrate metabolism, fatty acid oxidation, and muscle contraction proteins at 14 d postmortem.

The overall distribution of differentially abundant proteins in LL and PM muscles from 3 aging periods based on their functional clusters is presented in Figure 4. The identified proteins were related to

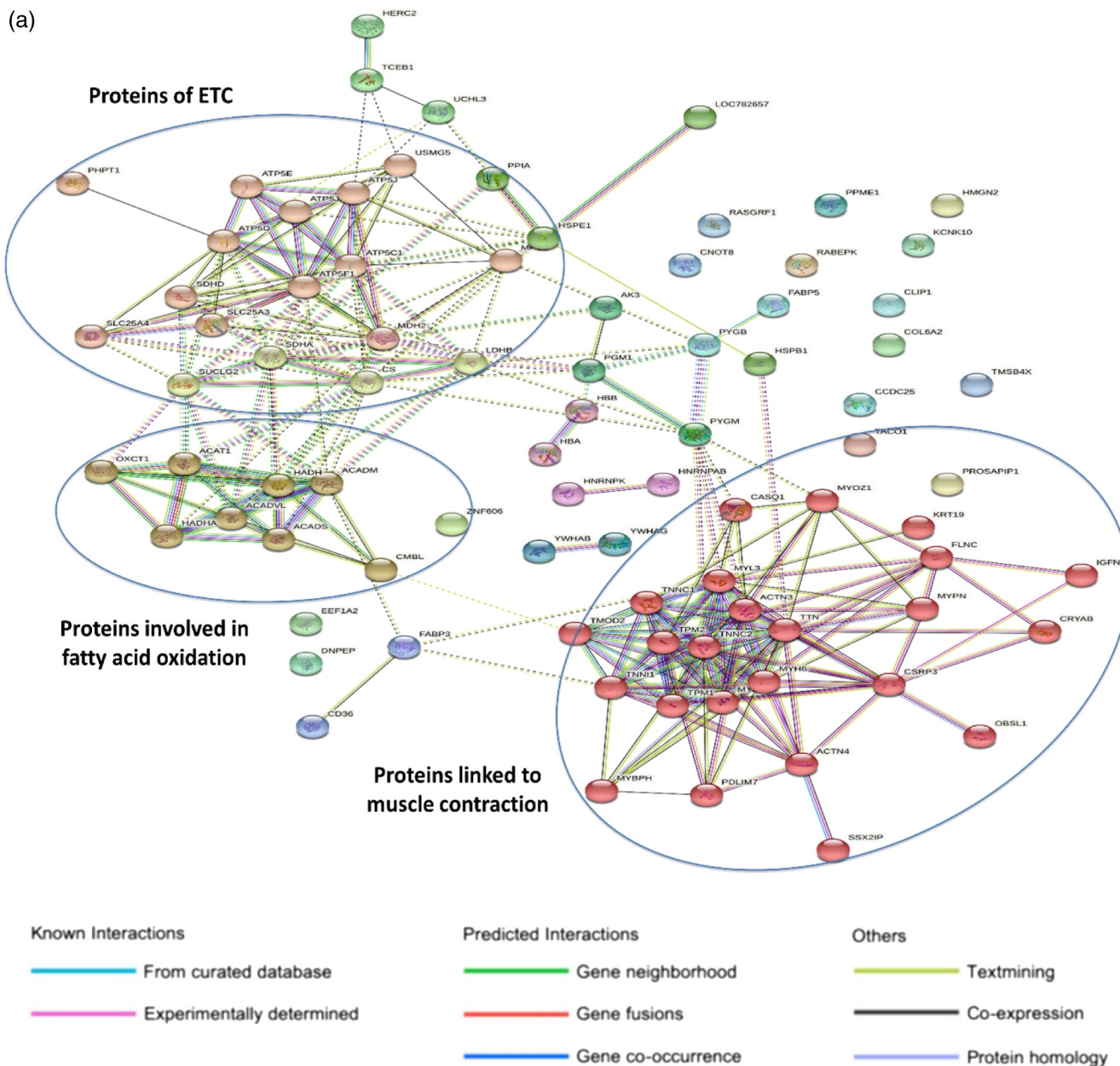


Figure 3. Protein–protein interaction networks of differential proteins between bison LL and PM muscles at aging periods of (3a) 2 d postmortem, (3b) 7 d postmortem and (3c) 14 d postmortem aging. (For more details on each protein and its function, please see the differentially abundant proteins listed in Table 1). LL = *longissimus lumborum*; PM = *psoas major*; ETC = electron transport chain

cytoskeleton (involved in both structure and muscle contraction), metabolic enzymes, chaperones, and cellular transportation. They were distributed differently at 3 aging periods. The overall changes in muscles’ biochemical and color attributes could be due to the metabolic enzymes (ETC, TCA cycle, fatty acid oxidation, and carbohydrate metabolism) at the 14-d postmortem period (31%); cytoskeletal proteins at the 2-d (24%), 7-d (32%), or 14-d (30%) postmortem periods; or transporter proteins (ATP and oxygen transport) at the 2-d (17%) postmortem period (Figure 4). The most

important differentially abundant proteins during comparisons of PM and LL at 2, 7, and 14 d postmortem and their expression patterns in ETC complexes are illustrated in Figure 5. It is clear from the figure that, at 2 d postmortem, proteins from complexes II and V of ETC were upregulated. In contrast, the upregulation of proteins from complexes II, IV, and V is found at 7 d, and upregulation of proteins from complexes II, III, IV, and V were noticed at 14 d postmortem. Moreover, a gradual involvement of a number of ETC complexes was also evident in the progression of 2-d (2), 7-d

(b)

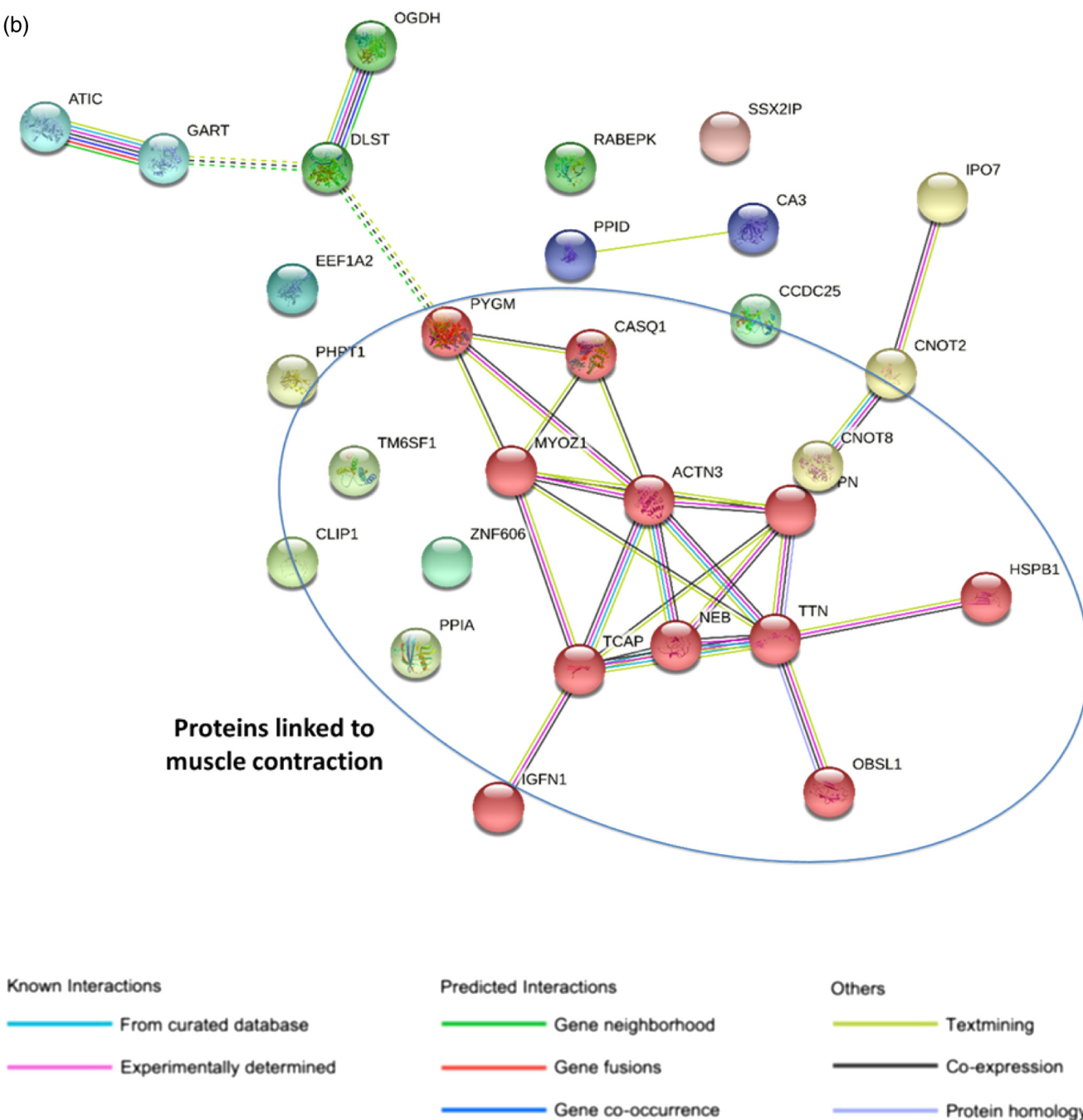


Figure 3. Continued.

(3), and 14-d (4) aging periods. These findings suggest that, at 14 d postmortem, the maximum number of ETC complexes and their associated proteins were activated and contributed to muscles’ oxidative changes. By investigating the protein–protein interaction networks at different aging periods when comparing PM and LL, some critical networks were explored using the IPA software and are presented in Figure 6. IPA is a very efficient tool for in-depth investigation of protein–protein interaction networks analysis.

In PM muscles at 2 d postmortem (Table 1), most of the identified differential proteins involved in ETC, fatty acid oxidation, TCA cycle, ATP and oxygen transport, and muscle contraction (50% proteins) exhibit increased expression when compared with LL. Similarly, in PM muscles at 7 d postmortem, fatty acid oxidation, ATP and oxygen transport, and muscle contraction proteins show increased expression levels compared with LL (Table 1). Furthermore, in PM muscles at 14 d postmortem, most of the proteins from

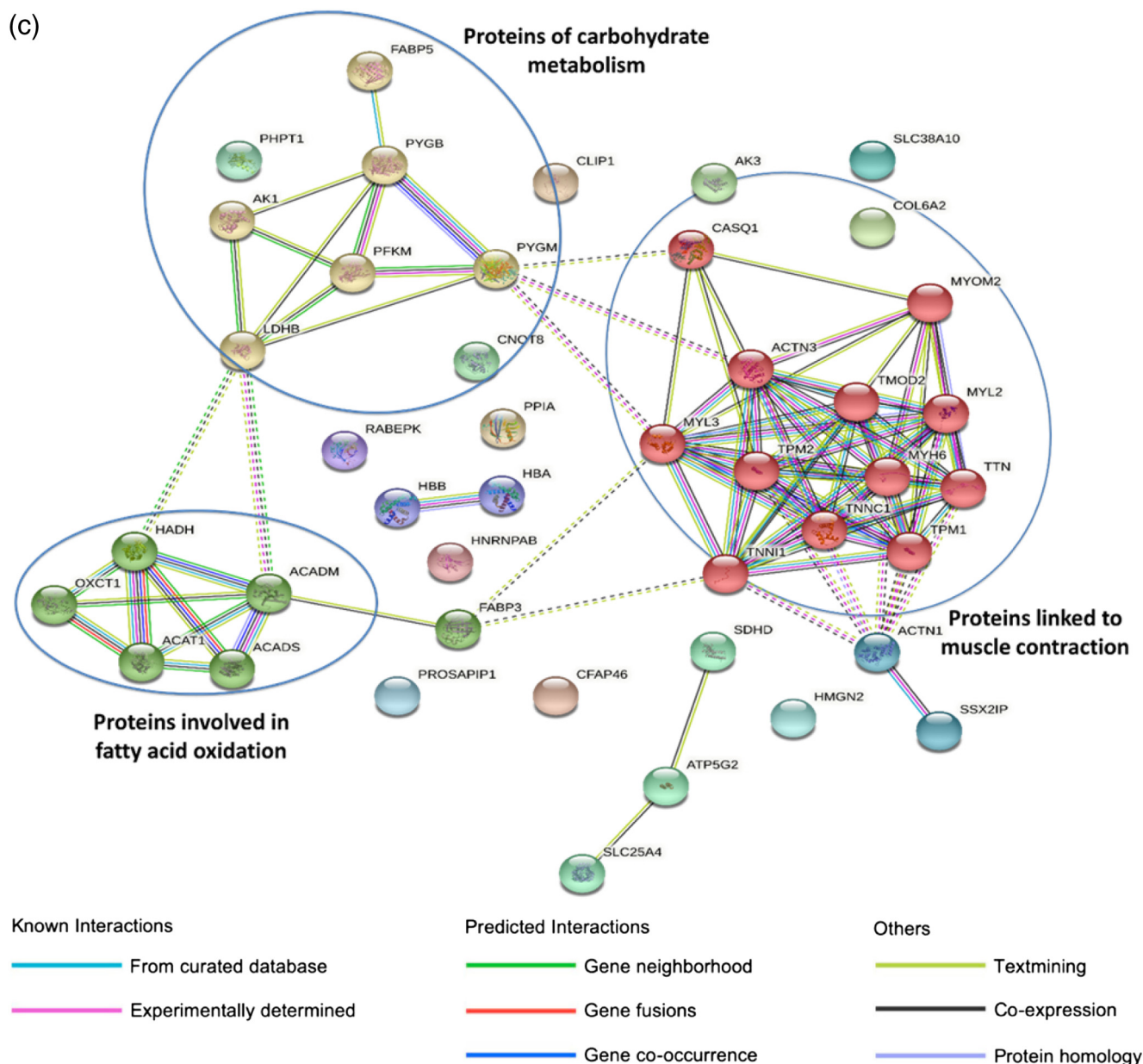


Figure 3. Continued.

fatty acid oxidation and oxygen transport, almost 50% of the muscle contraction proteins, few ETC proteins (2), and one ATP transport protein appear with increased expression levels compared with to LL (Table 1). However, the other protein groups exhibited different identification patterns. The differentially identified proteins presented in Table 1 are described subsequently in detail.

Enzymes involved in oxidative phosphorylation and ATP-transport proteins

In oxidative phosphorylation or ETC, 10 differential proteins were identified (Table 1) during

comparisons of LL and PM muscles from 3 aging periods. Among those proteins, succinate dehydrogenase cytochrome b small subunit (SDHD) and succinate dehydrogenase flavoprotein subunit (SDHA) were the component of mitochondrial complex II. Only one protein (cytochrome c) was part of mitochondrial complex IV that transfers electrons from cytochrome c molecules to dioxygen, resulting in the conversion of molecular oxygen into 2 water molecules (Li et al., 2006; Zhai et al., 2020). The other 7 differentially abundant proteins were the structural components of complex V (ATP synthase) and eventually involved in the ATP synthesis process. Among those, ATP synthase subunit gamma (ATP5C1), ATP synthase

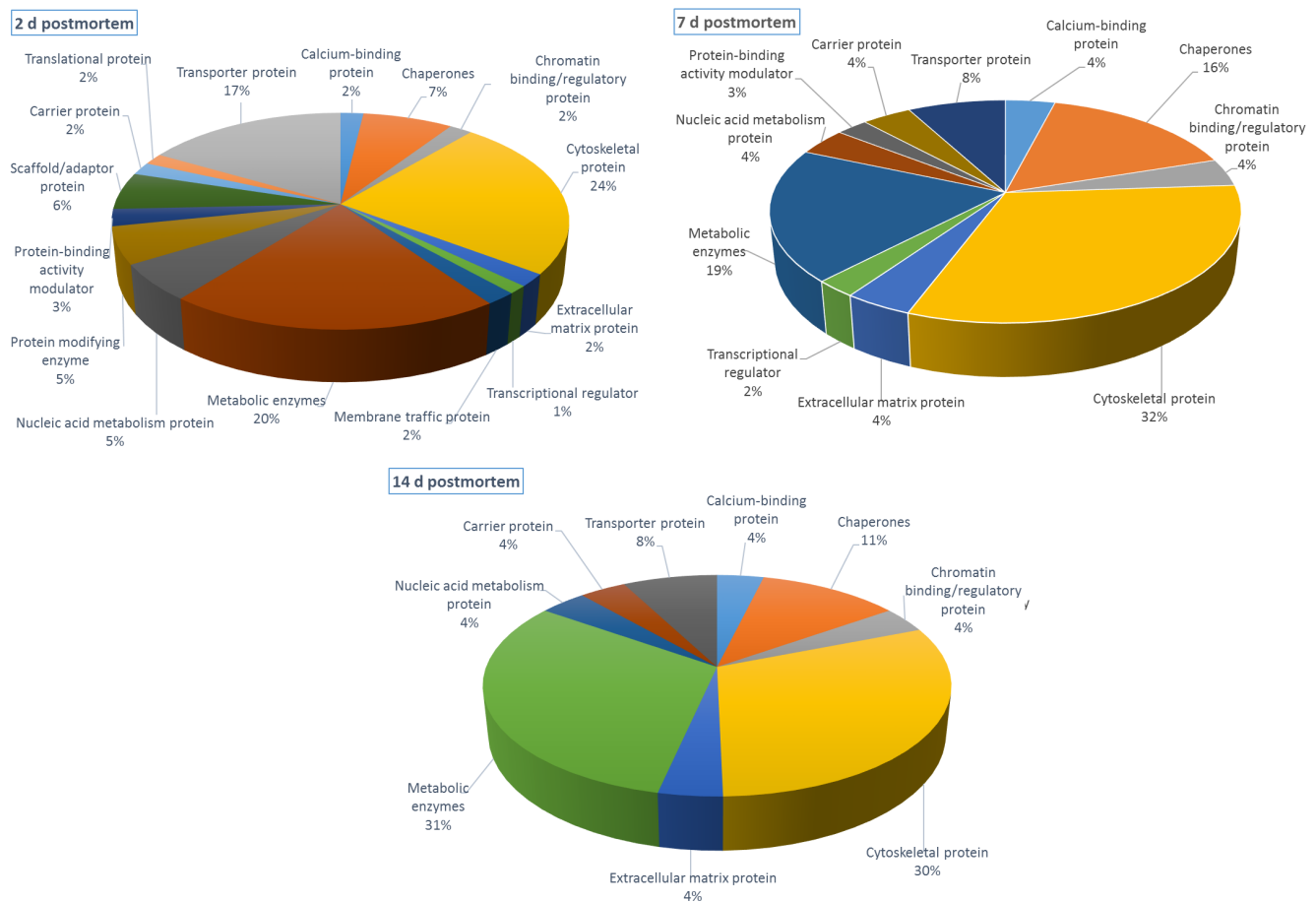


Figure 4. Distribution of the functional clusters of differential proteins between bison *longissimus lumborum* and *psoas major* muscles at 2-d, 7-d, and 14-d postmortem aging.

subunit delta (ATP5D), ATP synthase subunit epsilon (ATP5E), ATP synthase subunit f (ATP5J), and ATP synthesis-coupling factor 6 (ATP5J) were components of the F₁ part of complex V. ATP synthase subunit B1 (ATP5F) and ATP synthase subunit C2 (ATP5G2) were part of the F₀ portion of complex V. All these aforementioned proteins were found more abundant in PM muscles than in LL in each postmortem aging period. Also, 2 ATP-related transport proteins (Table 1), phosphate carrier protein (SLC25A3) and adenosine diphosphate (ADP)/ATP translocase 1 (SLC25A4), were identified as more abundant in PM muscles in almost all of the aging periods compared with LL.

TCA cycle and carbohydrate metabolism enzymes

Among the differential proteins in the TCA cycle (Table 1), citrate synthase (CS), malate dehydrogenase (MDH2), and succinyl-CoA ligase (SUCLG2) were identified as more abundant in PM muscles than in

LL mainly at 2 d postmortem. Related to carbohydrate metabolism enzymes, 5 proteins were reported as less abundant in PM muscles than LL: glycogen phosphorylase M (PYGM), glycogen phosphorylase B (PYGB), phosphoglycerate kinase 2 (PGK2), phosphoglucomutase-1 (PGM1), and ATP-dependent 6-phosphofructokinase (PFKM), at 2- and 14-d aging periods (Table 1).

Fatty acid oxidation enzymes

A total of 9 differential proteins (Table 1) linked to fatty acid degradation or β -oxidation were identified as more abundant in PM muscles at different aging periods compared with LL. Among those, 2 fatty acid-binding proteins (Fatty acid-binding protein, epidermal [FABP5] and Fatty acid-binding protein, heart [FABP3]) are actively involved in fatty acid catabolism, and binding and transporting fatty acids through cell membranes to mitochondria for oxidation (Zhai et al., 2020). Acetyl-CoA acetyltransferase mitochondrial isoform X1 (ACAT1) is involved in the reversible

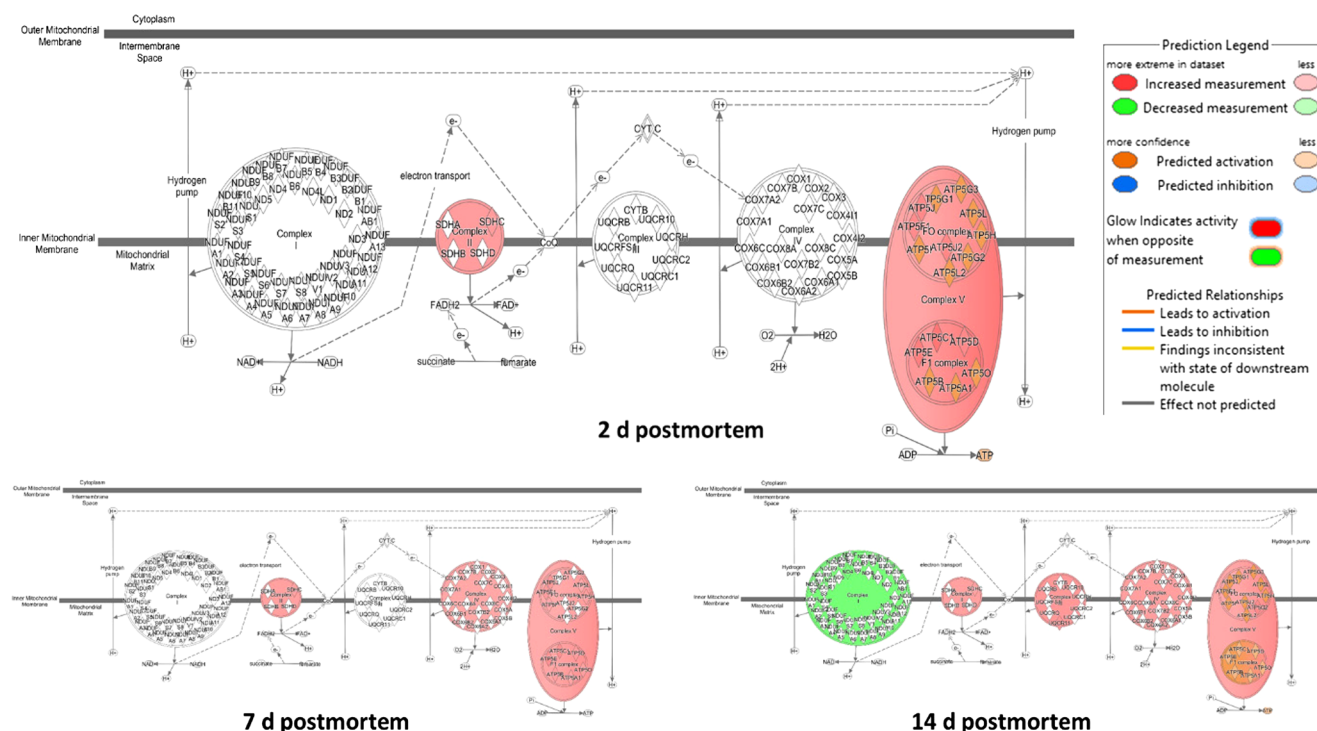


Figure 5. Complexes of ETC pathway affected during comparisons of bison PM vs. LL muscle at aging periods of 2-d, 7-d, and 14-d postmortem aging. LL = *longissimus lumborum*; PM = *psaos major*; ETC = electron transport chain

conversion of 2 acetyl-CoA to acetoacetyl-CoA and was reported more abundant in PM muscles (Zhai et al., 2020). Three proteins are also overexpressed in PM muscles compared with LL: long-chain specific acyl-CoA dehydrogenase (ACADVL), medium-chain specific acyl-CoA dehydrogenase (ACADM), and short-chain specific acyl-CoA dehydrogenase (ACADS) catalyze the first step of very long-chain, medium-chain, and short-chain fatty acids in the β -oxidation pathway, respectively (<http://www.uniprot.org/>; Zhai et al., 2020). Moreover, another enzyme—succinyl-CoA:3-ketoacid CoA transferase 1 (OXCT1), which is involved in the extrahepatic ketone body catabolism and energy supply (El Midaoui et al., 2005; Yu et al., 2017a)—was overexpressed in PM muscles compared with LL. Almost all of the aforementioned β -oxidation proteins were identified at all 3 aging periods.

Chaperone and oxygen-transport-related proteins

Among the 4 differentially identified chaperones (Table 1), 3 proteins showed decreased expression levels in PM muscles, such as peptidyl-prolyl cis-trans isomerase A (PPIA), heat shock 27 kDa protein (HSPB1), and alpha-crystallin B chain (CRYAB). In contrast, mitochondrial 10 kDa heat shock protein (HSPE1) exhibited increased expression in PM

compared with LL at 2 and 7 d postmortem. On the other hand, 2 major oxygen transport proteins (Table 1)—hemoglobin subunit alpha-I/II (HBA1) and hemoglobin subunit beta (HBB)—were detected as more abundant in PM muscles compared with LL at 2, 7, and 14 d postmortem.

Proteins with other functions

Among the other functions (Table 1), only antioxidant protein, namely glutathione S-transferase Mu 1-like (GSTM7), showed a lower expression pattern in PM muscles compared with LL. Moreover, the proteins involved in hydrolase activity—such as 14 kDa phosphohistidine phosphatase (PHPT1), carboxymethylenebutenolidase (CMBL), and aspartyl aminopeptidase isoform X1 (DNPEP)—also exhibited lower expression in PM than in LL. However, the proteins associated with demethylation protein phosphatase methyl esterase 1 isoform X1 (PPME1) and DNA binding non-histone chromosomal protein HMG-17 (HMGN2) showed upregulation patterns in PM muscles compared with LL. Almost all of the proteins described earlier were detected only at 2 d postmortem, except for HMGN2, which was identified at each aging period. The downregulation of GSTM7 antioxidant protein in PM muscles indicates that this muscle is more prone to oxidative damage resulting in less

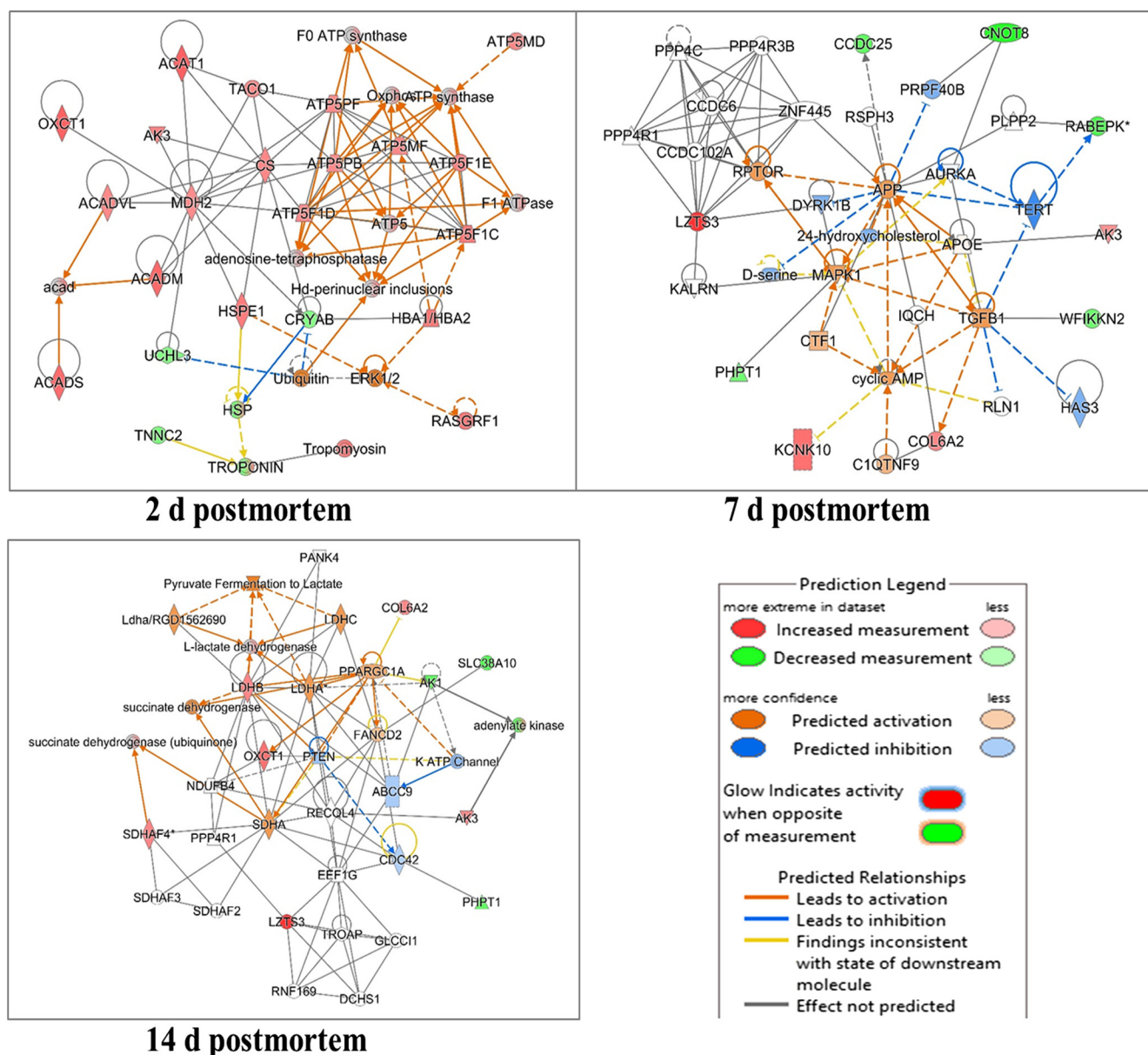


Figure 6. Major protein–protein interaction networks during comparisons of bison PM vs. LL muscle at 2-d, 7-d and 14-d postmortem identified using Ingenuity pathway analysis. (For more details on each protein and its function, please see the differentially abundant proteins listed in Table 1). LL = *longissimus lumborum*; PM = *psaos major*.

stability in color. A protein involved in purine metabolism, namely guanosine triphosphate (GTP):adenosine monophosphate (AMP) phosphotransferase AK3 (AK3), exhibited more expression in PM muscles than in LL at all 3 aging periods, whereas adenylate kinase 1 (AK1) showed less expression in PM only at 14-d aging time.

Proteins related to signal transduction such as kelch-like protein 41 (RABEPK↓), platelet glycoprotein 4/glycoprotein IIIB (CD36↑), ras-specific guanine nucleotide-releasing factor 1 (RASGRF1↑), protein ubiquitination E3 ubiquitin-protein ligase HERC2 isoform X1/HECT-type E3 ubiquitin transferase (HERC2↑), and ubiquitin carboxyl-terminal hydrolase

isozyme L3 (UCHL3↓), showed different (↓ = decreased and ↑ = increased) expression levels. Among these proteins, CD36 showed more expression in PM muscles at 2 d postmortem.

Proteins involved in muscle contraction and calcium signaling

Among muscle contraction-related proteins (Table 1), myosin regulatory light chain 2 (MYL2), myosin light chain 3 (MYL3), myosin-7 (MYH7), tropomyosin alpha-1 chain isoform X2 (TPM1), tropomyosin beta chain isoform X1 (TPM2), tropomyosin

Table 1. Differentially abundant proteins between bison PM and LL muscles at aging periods of 2 d, 7 d, and 14 d postmortem (fold change >1.5; $P < 0.05$)

Protein Description	Specific Function	Accession Number	Abbreviations (String Code)	Fold Change		
				PM vs. LL at 2 d	PM vs. LL at 7 d	PM vs. LL at 14 d
ETC/Oxidative Phosphorylation						
Succinate dehydrogenase (ubiquinone) cytochrome b small subunit, mitochondrial isoform X1	Complex II component and blocks generation of excess reactive O ₂	XP_010828629.1	SDHD	1.61		1.55
Succinate dehydrogenase (ubiquinone) flavoprotein subunit, mitochondrial	Complex II component and metal ion binding	XP_010830641.1	SDHA	1.53		
Cytochrome c	Complex III and IV component, heme and metal ion binding	XP_010853678.1	TACO1 (LOC104999778)	1.58		
ATP synthase subunit gamma, mitochondrial isoform X1	Complex V component and ATP synthesis	XP_010851442.1	ATP5C1	1.79		
ATP synthase subunit delta, mitochondrial	Proton transportation and ATP synthase activity	XP_010842883.1	ATP5D	1.55		
ATP synthase subunit epsilon, mitochondrial	Complex V component, hydrogen ion transport, and ATP synthesis	XP_010837454.1	ATP5E	1.67		
ATP synthase F(0) complex subunit B1, mitochondrial	Complex V component and ATP synthesis	XP_010829138.1	ATP5F1	1.52		
ATP synthase F(0) complex subunit C2, mitochondrial	Complex V component and ATP synthesis	XP_010831422.1	ATP5G2			1.53
ATP synthase-coupling factor 6, mitochondrial	ATP synthesis coupled proton transport	XP_010836757.1	ATP5J	1.55		
ATP synthase subunit f, mitochondrial	Complex V component, hydrogen ion transport, and ATP synthesis	XP_010844025.1	ATP5J2	1.58		
TCA Cycle						
Citrate synthase, mitochondrial isoform X1	Citric acid synthesis	XP_010837550.1	CS	1.58		
Malate dehydrogenase, mitochondrial	NADH production	XP_010852621.1	MDH2	1.53		
Succinyl-CoA ligase, subunit beta, mitochondrial	GTP production	XP_010852852.1	SUCLG2	1.82	1.52	
Mitochondrial pyruvate carrier 2	Mitochondrial uptake of pyruvate, pyruvate transport	XP_010844313.1	MPC2	1.74		
2-oxoglutarate dehydrogenase, mitochondrial isoform X1	TPP binding and oxidoreductase activity	XP_010827341.1	OGDH		-1.51	
ATP Transport Related						
Phosphate carrier protein, mitochondrial isoform X1	Transmembrane phosphate carrier	XP_010829873.1	SLC25A3	1.71	1.52	1.59
ADP/ATP translocase 1	Catalyzes the exchange of ADP and ATP across the membrane	XP_010834070.1	SLC25A4	1.84	1.61	
Transporter/Carrier Proteins						
Potassium channel subfamily K member 10	Transporter or carrier proteins (K ion channel binding)	XP_010843536.1	KCNK10	1.99	1.95	
Thiosulfate sulfurtransferase	Cellular transport, detoxification, and transferase activity	XP_010858855.1	TSTD3	1.95		
Putative sodium-coupled neutral amino acid transporter 10 isoform X1	Membrane component and neutral amino acid transport	XP_010854613.1	SLC38A10			-1.67

Table 1. (Continued)

Protein Description	Specific Function	Accession Number	Abbreviations (String Code)	Fold Change		
				PM vs. LL at 2 d	PM vs. LL at 7 d	PM vs. LL at 14 d
Carbohydrate Metabolism						
Glycogen phosphorylase, muscle form	Glycogen catabolism	XP_010836307.1	PYGM	−1.79	−1.77	−2.19
Glycogen phosphorylase, brain form	Glycogen catabolism	XP_010834913.1	PYGB	−1.53		−1.62
Phosphoglycerate kinase 2	ATP utilization	XP_010861335.1	PGK2	−1.53		
Phosphoglucomutase-1 isoform X2	Magnesium binding	XP_010832195.1	PGM1	−1.56		
ATP-dependent 6-phosphofructokinase, muscle type	ATP binding and utilization	XP_010835801.1	PFKM			−1.75
L-lactate dehydrogenase	Lactate to pyruvate conversion and NADH production	XP_010854247.1	LDHB	1.73		1.54
Lipid Metabolism/Fatty Acid Oxidation						
Fatty acid-binding protein, heart	Fatty acid binding and inhibit cell growth	XP_010835191.1	FABP3	2.33	1.93	1.82
Fatty acid-binding protein, epidermal	Fatty acid binding and transport	XP_010861708.1	FABP5	1.74	1.57	1.60
Acetyl-CoA acetyltransferase, mitochondrial isoform X1	Beta oxidation	XP_010861136.1	ACAT1	2.10	1.69	1.65
Succinyl-CoA:3-ketoacid coenzyme A transferase 1, mitochondrial	Ketone body metabolism	XP_010852017.1	OXCT1	2.07	1.82	1.80
Very long-chain specific acyl-CoA dehydrogenase, mitochondrial isoform X1	Beta oxidation, FAD binding, and dehydrogenase	XP_010845646.1	ACADVL	1.56		
Medium-chain specific acyl-CoA dehydrogenase, mitochondrial	Beta oxidation, FAD binding, and dehydrogenase	XP_010856422.1	ACADM (LOC105001724)	1.97	1.67	1.67
Short-chain specific acyl-CoA dehydrogenase, mitochondrial isoform X1	Beta oxidation, FAD binding, and oxidoreductase activity	XP_010826938.1	ACADS	1.93	1.65	1.64
Hydroxyacyl-coenzyme A dehydrogenase, mitochondrial	NAD/NADP binding and oxidoreductase activity	XP_010856864.1	HADH	1.82	1.59	1.56
Enoyl-CoA hydratase	Beta oxidation, NADH production	XP_010838888.1	HADHA	1.57		
Muscle Contraction						
Myosin regulatory light chain 2	Calcium ion binding	XP_010839683.1	MYL2	1.88	1.93	1.85
Myosin light chain 3	Calcium ion binding	XP_010860678.1	MYL3	3.73	2.83	2.33
Myosin-7	Calcium ion binding	XP_010829714.1	MYH7	2.73	2.50	2.62
Tropomyosin alpha-1 chain isoform X2	Actin binding	XP_010831764.1	TPM1	1.66	1.55	
Tropomyosin alpha-3 chain isoform X1	Actin binding	XP_010836667.1	TPM3	1.95	1.72	1.85
Tropomyosin beta chain isoform X1	Actin binding	XP_010844389.1	TPM2	1.79	1.80	1.79
Tropomodulin-2 isoform X1	Tropomyosin binding	XP_010837785.1	TMOD2	1.75	2.22	1.80
Troponin C, slow skeletal muscle	Calcium ion binding	XP_010850036.1	TNNC1	1.62		1.67
Troponin I, slow skeletal muscle	Prevents muscle contraction	XP_010829410.1	TNNI1	1.62		1.54
Thymosin beta-4	Actin binding	XP_010828621.1	TMSB4X	1.56		

Table 1. (Continued)

Protein Description	Specific Function	Accession Number	Abbreviations (String Code)	Fold Change		
				PM vs. LL at 2 d	PM vs. LL at 7 d	PM vs. LL at 14 d
Upregulated during skeletal muscle growth protein 5	Transmembrane protein	XP_010857721.1	USMG5	1.56		
Troponin C, skeletal muscle	Calcium ion binding	XP_010833333.1	TNNC2	-1.68		
Coiled-coil domain-containing protein 25	Receptor protein and cytoskeleton rearranges during cell motility	XP_010837897.1	CCDC25	-1.87	-1.74	
Myosin-binding protein H	Myosin binding	XP_010852420.1	MYBPH	-1.51		
Alpha-actinin-1 isoform X1	Actin and calcium binding	XP_010845002.1	ACTN1			-1.53
Alpha-actinin-3	Actin and calcium binding	XP_010836049.1	ACTN3 (LOC104986993)	-2.45	-1.96	-1.79
Alpha-actinin-3-like	Actin binding	XP_010836047.1	SSX2IP (LOC104986992)	-2.19	-1.85	-1.62
Alpha-actinin-4	Actin and calcium binding	XP_010847616.1	ACTN4	-1.56		
Obscurin	Muscle structure, cell adhesion, and ATP binding	XP_010845591.1	OBSL1	-1.58		
14-3-3 protein beta/alpha	Muscle structure, signal transduction	XP_010839277.1	YWHAB	-1.59		
14-3-3 protein gamma	Muscle structure	XP_010852658.1	YWHAG	-1.62		
Myozenin-1	Actin and Z disc binding	XP_010850615.1	MYOZ1	-1.95	-1.66	
Myomesin-2	Actin and kinase binding	XP_010833576.1	MYOM2			-1.52
Myopalladin isoform X1	Actin binding and sarcomere organization	XP_010850458.1	MYPN	-2.85	-2.25	
LOW QUALITY PROTEIN: immunoglobulin-like and fibronectin type III domain-containing protein 1	Serine protease inhibitor (metalloendopeptidase inhibitor)	XP_010829429.1	IGFN1(WFIKKN2)	-1.67	-1.58	
Calcium Signalling						
Calsequestrin-1	Calcium storage and binding	XP_010845176.1	CASQ1	-2.14	-1.82	-1.58
Protein S100-A1	Calcium binding	XP_010836708.1	S100A1		-1.53	
Muscle Structure Components						
Leucine zipper putative tumor suppressor 3 isoform X1	Cell cycle (cell growth prevention)	XP_010834798.1	LZTS3 (LOC104986066)	5.82	6.19	4.82
Collagen alpha-2(VI) chain	Muscle structure, connective tissue	XP_010833290.1	COL6A2	1.59	1.66	1.52
PDZ and LIM domain protein 7 isoform X3	Protein-protein interaction	XP_010844848.1	PDLIM7	-1.72		
Protein CFAP46, partial	Muscle structure and motility	XP_010857855.1	CFAP46			-1.69
CAP-Gly domain-containing linker protein 1 isoform X1	Muscle structure	XP_010839621.1	CLIP1	-2.68	-2.41	-1.99
LOW QUALITY PROTEIN: filamin-C	Muscle structure	XP_010830065.1	FLNC	-1.59		
LOW QUALITY PROTEIN: keratin, type I cytoskeletal 14-like	Muscle structure	XP_010840848.1	KRT14 (LOC104990465)	-1.59		
LOW QUALITY PROTEIN: titin	Muscle structure and ATP binding	XP_010858056.1	TTN	-1.93	-1.79	-1.67
Chaperones						
Peptidyl-prolyl cis-trans isomerase A	Protein folding and MAPK/ERK activation	XP_010829539.1	PPIA (LOC104981978)	-1.83	-1.87	-2.10
Heat shock 27 kDa protein	Protein folding, actin organization, and stress resistance	XP_010852626.1	HSPB1	-1.79	-1.52	
Alpha-crystallin B chain	Chaperone-like activity in stress condition	XP_010861174.1	CRYAB	-1.58		

Table 1. (Continued)

Protein Description	Specific Function	Accession Number	Abbreviations (String Code)	Fold Change		
				PM vs. LL at 2 d	PM vs. LL at 7 d	PM vs. LL at 14 d
10 kDa heat shock protein, mitochondrial	Protein folding, ATP binding, and ATPase activity	XP_010859205.1	HSPE1	1.73	1.55	
Oxygen Transport						
Hemoglobin subunit alpha-I/II	Heme and O ₂ binding, and H ₂ O ₂ detoxification	XP_010855734.1	HBA1 (LOC105001245)	1.82	1.88	1.79
Hemoglobin subunit beta	Heme, metal ion and O ₂ binding	XP_010830570.1	HBB	1.82	1.95	1.74
Protein Synthesis						
<i>Transcription</i>						
CCR4-NOT transcription complex subunit 3-like	Transcription repression	XP_010834567.1	CNOT8 (LOC104985867)	-3.07	-2.66	-2.13
Zinc finger protein 606 isoform X2	Transcription regulation by binding RNA polymerase II	XP_010855944.1	ZNF606 (LOC105001395)	-1.75	-1.59	
Heterogeneous nuclear ribonucleoprotein K isoform X1	Transcription regulation, DNA and RNA binding, repressor	XP_010838359.1	HNRNPK	-1.52		
Cysteine and glycine-rich protein 3	Positive modulator/cofactor for myogenic transcription factor MYOD1	XP_010856729.1	CSRP3	-1.92		
Transcription elongation factor B polypeptide 1	Ubiquitin-dependent catabolic protein, protein synthesis, translation	XP_010845244.1	TCEB1	-1.71		
Heterogeneous nuclear ribonucleoprotein A/B	RNA binding and transcription termination	XP_010844805.1	HNRNPAB	1.65		1.69
<i>Translation</i>						
Elongation factor 1-alpha 2	Protein biosynthesis, GTP binding, translation	XP_010834950.1	EEF1A2	-1.52		
Eukaryotic translation initiation factor 5A-1	Translation initiation, elongation, protein synthesis and transport	XP_010845638.1	EIF5AL1	-1.56		
Other Functions						
<i>Antioxidant</i>						
Glutathione S-transferase Mu 1-like	Neutralizes reactive oxygen species	XP_010829201.1	GSTM7 (LOC104981668)	-1.61		
<i>Hydrolases</i>						
14 kDa phosphohistidine phosphatase, partial	Histidine phosphatase	XP_010852119.1	PHPT1	-1.83	-1.54	-1.51
	Carboxymethylenebutenolidase homolog	Cysteine hydrolase	XP_010845828.1	CMBL	-1.51	
Aspartyl aminopeptidase isoform X1	Aminopeptidase, metalloproteinase, zinc binding	XP_010859551.1	DNPEP	-3.18		
<i>Purine Metabolism</i>						
GTP:AMP phosphotransferase AK3, mitochondrial isoform X1	ATP and GTP binding and adenylate kinase activity	XP_010859018.1	AK3	1.62	1.51	1.51
Adenylate kinase isoenzyme 1	ATP binding and utilization	XP_010855189.1	AK1			-1.53
Bifunctional purine biosynthesis protein PURH	Purine biosynthesis, transferase, and IMP synthase activity	XP_010859447.1	ATIC		-1.53	
<i>Demethylation</i>						
Protein phosphatase methyl esterase 1 isoform X1	Protein demethylation	XP_010847156.1	PPME1	1.60		
<i>DNA Binding</i>						
Non-histone chromosomal protein HMG-17	Nucleosomal DNA binding	XP_010828409.1	HMGN2	1.59	1.60	1.56

Table 1. (Continued)

Protein Description	Specific Function	Accession Number	Abbreviations (String Code)	Fold Change		
				PM vs. LL at 2 d	PM vs. LL at 7 d	PM vs. LL at 14 d
<i>Protein Ubiquitination</i>						
E3 ubiquitin-protein ligase HERC2 isoform X1/ HECT-type E3 ubiquitin transferase	Protein ubiquitination and modification	XP_010851284.1	HERC2 (LOC104997998)	1.59		
Ubiquitin carboxyl-terminal hydrolase isozyme L3	Ubiquitin-dependent protein catabolism, peptidase, esterase, and amidase activity	XP_010837967.1	UCHL3	−1.55		
<i>Signal Transduction</i>						
Kelch-like protein 41	Regulation of Rac protein signal transduction and cell motility	XP_010847693.1	RABEPK	−2.23	−1.96	−1.64
Platelet glycoprotein 4/ glycoprotein IIIB	Cell signalling, immune response, and lipid utilization	XP_010846409.1	CD36 (LOC104994511)	1.56		
LOW QUALITY PROTEIN: ras-specific guanine nucleotide-releasing factor 1	Small GTPase-mediated signal transduction and regulation of Rho protein	XP_010841694.1	RASGRF1	1.85		

ADP = adenosine diphosphate; AMP = adenosine monophosphate; ATP = adenosine triphosphate; CS = citrate synthase; ETC = electron transport chain; FABP3 = Fatty acid-binding protein, heart; FABP5 = Fatty acid-binding protein, epidermal; GTP = guanosine triphosphate; HMG2 = non-histone chromosomal protein HMG-17; LDHB = L-lactate dehydrogenase; MPC2 = mitochondrial pyruvate carrier 2; NADH = nicotinamide adenine dinucleotide; OGDH = 2-oxoglutarate dehydrogenase mitochondrial isoform X1; PPME1 = protein phosphatase methyl esterase 1 isoform X1; TCA = tricarboxylic acid cycle; LL = *longissimus lumborum*; PM = *psaos major*.

alpha-3 chain isoform X1 (TPM3), tropomodulin-2 isoform X1 (TMOD2), troponin C (slow skeletal muscle; TNNC1), troponin I (slow skeletal muscle; TNNI1), thymosin beta-4 (TMSB4X), and upregulated during skeletal muscle growth protein 5 (USMG5) showed increase expression in PM muscles compared with LL at almost all 3 aging periods.

On the other hand, troponin C (TNNC2), coiled-coil domain-containing protein 25 (CCDC25), myosin-binding protein H (MYBPH), alpha-actinin-1 (ACTN1), alpha-actinin-3 (ACTN3), alpha-actinin-3-like (SSX2IP), alpha-actinin-4 (ACTN4), obscurin (OBSL1), 14-3-3 protein beta/alpha (YWHAB), 14-3-3 protein gamma (YWHAG), myozenin-1 (MYOZ1), myomesin-2 (MYOM2), myopalladin isoform X1 (MYPN), and immunoglobulin-like and fibronectin type III domain-containing protein 1 (IGFN1) were identified less abundances in PM muscles than in LL (Table 1) at 2 d postmortem. Two proteins from the calcium signaling pathway—calsequestrin-1 (CASQ1) and protein S100-A1 (S100A1)—were found to be downregulated in PM muscles in comparison with LL (Table 1). CASQ1 was detected at all 3 aging times, whereas S100A1 was identified only at 7 d postmortem.

Muscle structure components

Eight proteins associated with muscle structure showed different abundance levels in LL and PM muscles (Table 1). Among those, leucine zipper

putative tumor suppressor 3 (LZTS3) and collagen alpha-2(VI) chain (COL6A2) are components of the cell cycle and connective tissue. They exhibited increased expression in PM compared with LL at all 3 aging times. On the other hand, PDZ and LIM domain protein 7 (PDLIM7), protein CFAP46 (CFAP46), CAP-Gly domain-containing linker protein 1 (CLIP1), filamin-C (FLNC), keratin type I cytoskeletal 14-like (KRT14), and titin (TTN) were expressed in decreased levels in PM relative to LL, with different identification patterns at the 3 aging periods.

Proteins involved in protein synthesis

Most differential proteins identified from the transcription (Table 1) process, including CCR4-NOT transcription complex subunit 3-like (CNOT8), zinc finger protein 606 (ZNF606), heterogeneous nuclear ribonucleoprotein K (HNRNPK), cysteine and glycine-rich protein 3 (CSRP3), and transcription elongation factor B polypeptide 1 (TCEB1), were downregulated in PM muscles compared with in LL. However, only heterogeneous nuclear ribonucleoprotein A/B (HNRNPAB) from the aforementioned group showed a pattern of upregulation in PM compared with LL muscles (Table 1). Two translation process-associated proteins (elongation factor 1-alpha 2 [EEF1A2] and eukaryotic translation initiation factor 5A-1 [EIF5AL1]) showed decreased expression in PM muscles compared

with LL. Almost all of the previously described proteins were detected at 2 d postmortem.

DISCUSSION

Enzymes involved in oxidative phosphorylation and ATP-transport proteins

Ten differential oxidative phosphorylation or ETC proteins were found to be more abundant in PM muscles than in LL in each postmortem aging period. Those proteins increase the rates of oxygen consumption in mitochondria (O’Keeffe and Hood, 1982; McKenna et al., 2005; Yu et al., 2017b, 2018; Zhai et al., 2020). These studies support our presented results. On the other hand, ATP-related transport proteins such as SLC25A3 and SLC25A4 are responsible for transmembrane phosphate transport and exchange of ADP/ATP across the membrane, respectively, which could contribute to the higher production of ATP (Zhai et al., 2020) and regulate the permeability of mitochondria (Yu et al., 2018). In the current study, these proteins were abundant in PM muscles, which could enhance oxidative phosphorylation enzyme function (Yu et al., 2017b, 2018; Zhai et al., 2020). Furthermore, the ETC and ATP transport occur in mitochondria and related proteins are connected within the same protein–protein interaction cluster (Figure 3a) at 2 d postmortem and thus participate in oxidative phosphorylation reactions together.

Generally in ETC, complex I (Turrens and Boveris, 1980; Genova et al., 2001; Kushnareva et al., 2002), complex II (Quinlan et al., 2012), and complex III (Dröse and Brandt, 2008) can generate reactive oxygen species (ROS) in the course of oxidative phosphorylation reactions. These ROS can directly damage complex I–IV (Brown, 1999) and SLC25A4 (Yan and Sohal, 1998), which can consequently initiate signal transduction, resulting in cell death (Vakifahmetoglu-Norberg et al., 2017). Therefore, ROS-producing proteins found overabundant in PM muscles relative to LL indicate more oxidative stress, release of cytochrome c, and quick degradation of mitochondria in PM, confirming this muscle as color labile compared with LL in early display periods (Ke et al., 2017; Mancini et al., 2018).

TCA cycle and carbohydrate metabolism enzymes

Among the differential proteins in the TCA cycle, CS, MDH2, and SUCLG2 were more abundant in PM

muscles compared with LL (Yu et al., 2017b, 2018; Ramanathan et al., 2021). These proteins contribute to the production of ATP by oxidative phosphorylation in PM muscles, resulting in the production of ROS and, consequently, oxidative and color instability. Another protein, mitochondrial pyruvate carrier 2 (MPC2), is responsible for the uptake of pyruvate in mitochondria, which ultimately enters into the TCA cycle after converting to acetyl-CoA and contributes to the production of nicotinamide adenine dinucleotide (NADH) and other reducing equivalents, also fed into ETC for ATP production. On the other hand, PM muscle contains greater amounts of Mb and mitochondria, resulting in more oxygen utilization in PM compared with LL (Hwang et al., 2010; Canto et al., 2016). Therefore, these TCA cycle enzymes (Yu et al., 2017b, 2018; Zhai et al., 2020) can contribute to higher consumption of oxygen in oxidative metabolism (O’Keeffe and Hood, 1982; McKenna et al., 2005) and ROS generation, inducing stress in postmortem PM muscles, which consequently leads to lower metmyoglobin reducing activity (MRA) and increased discoloration in PM (Ramanathan et al., 2019).

NADH is a crucial component of enzymatic and nonenzymatic MRA (Echevarne et al., 1990; Mancini and Hunt, 2005; Kim et al., 2006; Ramanathan et al., 2021) and MPC2 protein, could contribute to the production of reducing equivalents, including NADH. At the same time, 2-oxoglutarate dehydrogenase mitochondrial isoform X1 (OGDH) plays a role in catalytic conversion of 2-oxoglutarate to succinyl-CoA, CO₂, and NADH (Qi et al., 2011; Zhai et al., 2019). The less abundance of OGDH in PM muscles could lead to less MRA, resulting in lower color stability (Ramanathan et al., 2020a, 2020b).

Previous studies also confirmed the lower abundance of glycolytic enzymes in PM muscles than in LL, resulting in negative effects on color attributes (Hunt and Hedrick, 1977; Kirchofer et al., 2002; Joseph et al., 2012; Mancini et al., 2018; Ramanathan and Mancini, 2018; Yu et al., 2018). However, L-lactate dehydrogenase (LDHB), which converts lactate to pyruvate in the anaerobic glycolysis process and generates NADH, was identified as more abundant in PM muscles compared with LL. Nevertheless, as oxidative phosphorylation was dominant in PM muscles, this NADH could be mainly utilized by ETC for producing ATP rather than involved in other reduction processes such as MRA. As a result, the presence of LDHB was not effective enough for maintaining the oxidative and color stability in PM muscles.

Fatty acid oxidation enzymes

In PM muscles, more fatty acid oxidation enzymes than in LL could be the reflection of elevated lipid oxidation. In agreement with this view, previous studies reported more lipid oxidation in PM compared with LL (Canto et al., 2015; Hasan et al., 2021). Other studies also demonstrated more β -oxidation enzymes in PM than LL (Yu et al., 2018; Zhai et al., 2020) during postmortem aging. One interaction cluster including fatty acid oxidation proteins was detected both at 2 d (Figure 3a) and at 14 d (Figure 3c), emphasizing the contributions of β -oxidation to the oxidative processes that occurred within the postmortem bison muscles. Therefore, the overabundance of fatty acid oxidation enzymes in PM muscles indicates more oxidative stress, resulting in the production of ROS and deterioration of color in PM (Zhai et al., 2020) in combination with overexpression of the TCA cycle and oxidative phosphorylation enzymes.

Chaperone and oxygen-transport-related proteins

In PM muscles, PPIA, HSPB1 and CRYAB showed decreased expression, whereas HSPE1 exhibited increased expression in PM compared with LL. PPIA plays a prominent role in the survival of cells (Obchoei et al., 2009; Cheng et al., 2016) by minimizing the cellular damage caused by ROS (Doyle et al., 1999; Lee et al., 2001; Suzuki et al., 2006; Kyu et al., 2007). HSPE1 is involved in mitochondrial protein import and macromolecular structure assembly, subsequently contributing to protein folding in association with HSP60 (Maciel et al., 2020). Although, HSPE1 was more abundant in PM muscles, this protein may have functions other than chaperone activity. Generally, chaperones are involved in the covalent folding or unfolding of protein structures and consequently minimize the cellular stress (Zhai et al., 2020). The lower expression of most of the identified chaperones in PM muscles is an indication of higher stress levels, ROS production, and consequently accelerated color deterioration relative to LL.

Oxygen transporters HBA1 and HBB were detected as upregulated in PM muscles compared with LL, which is in agreement with previous studies (Yu et al., 2017b; Zhai et al., 2020). The presence of more hemoglobin subunits in PM muscle makes it highly vulnerable to autoxidation, owing to the oxidative-stress-induced lipid oxidation and consequently lower stability of color in PM muscles compared with LL (Misra and Fridovich, 1972; Sadrzadeh et al.,

1984; Moxness et al., 1996; Olsson et al., 2010; Canto et al., 2016).

Proteins with other functions

Antioxidant proteins such as GSTM7, PHPT1, CMBL, and DNPEP exhibited lower expression in PM than in LL. GSTM7 mainly belongs to the glutathione S-transferase (GST) superfamily and neutralizes the cellular ROS and protects cells from oxidative stress and damage (Zhao et al., 2010; Oakley, 2011). The downregulation of GSTM7 in PM muscles may indicate that this muscle is more prone to oxidative damage resulting in less stability in color. Among other proteins, AK3 can generate AMP from ADP, and AMP in turn is related to the signalling cascade linked to cellular damage (Dzeja and Terzic, 2009; Panayiotou et al., 2014; Zhai et al., 2020). In contrast, the overabundance of the AK1 protein was found to be linked to the stability of color in fresh beef (Canto et al., 2015). Signal transduction proteins such as CD36 showed more expression in PM muscles, and this protein is involved in the immune response, cell signalling, and lipid oxidation (<http://www.uniprot.org/>) and thus could contribute to color deterioration in PM muscles, especially by exerting its effect on the lipid oxidation process.

Proteins involved in muscle contraction, calcium signaling, muscle structure components, and protein synthesis

Most of those proteins were more abundant in PM muscles compared with LL ($P > 0.05$). Among those groups, muscle contraction proteins showed protein-protein interaction networks at all 3 aging times (Figure 3), indicating that these proteins could have significant roles in the postmortem changes in bison muscles. However, their impact on color stability has not been reported, according to the author's knowledge, and needs to be investigated.

Conclusions

In summary, based on the overall results, the enzymes involved in oxidative metabolism contributed to oxidative stress as well as color instability in bison PM muscles by producing ROS. Increased expression of both ATP producing and transport-related proteins in PM muscles also contributed to oxidative instability, which could be reflected in meat color instability. To the best of our knowledge, this study is the first

to report most of the proteins involved in muscle contraction, calcium signaling, muscle structure components, and protein synthesis, as well as antioxidant, hydrolase, demethylation, protein binding, and DNA ubiquitination in bison muscles compared with other proteome studies on cattle. However, their impact on color stability needs to be investigated. Therefore, this isobaric tag-based TMT analysis was successful in uncovering the variations in sarcoplasmic proteomes of 2 major bison muscles (LL and PM), resulting in discrimination among those muscles with inherent color stability.

Acknowledgments

The authors are grateful for and highly appreciate the funding support from the Natural Sciences and Engineering Research Council (NSERC Discovery Grants Program #RGPIN-2016-06006) to complete this research.

Literature Cited

- Aalhus, J. L., W. M. Robertson, and J. Ye. 2009. Muscle fiber characteristics and their relation to meat quality. In: M. Du and R. J. McCormick, editors, *Applied muscle biology and meat science*. pp. 97–114. <https://doi.org/10.1201/b15797-9>.
- Alderton, A. L., C. Faustman, D. C. Liebler, and D. W. Hill. 2003. Induction of redox instability of bovine myoglobin by adduction with 4-hydroxy-2-nonenal. *Biochemistry*. 42:4398–4405. <https://doi.org/10.1021/bi0271695>.
- Bradford, M. M. 1976. A rapid and sensitive method for the quantitation of microgram quantities of protein utilizing the principle of protein-dye binding. *Anal. Biochem.* 72:248–254. <https://doi.org/10.1006/abio.1976.9999>.
- Brown, G. C. 1999. Nitric oxide and mitochondrial respiration. *BBA-Bioenergetics*. 1411:351–369. [https://doi.org/10.1016/S0005-2728\(99\)00025-0](https://doi.org/10.1016/S0005-2728(99)00025-0).
- Canada Gazette. 1992. Part II: Livestock and poultry carcass grading regulations. Part III. Grade names and grade standards for beef carcasses. Government of Canada. <https://laws-lois.justice.gc.ca/eng/regulations/SOR-92-541/20070503/P1TT3xt3.html>. (Updated 14 January 2019; Accessed 6 February 2022).
- Canto, A. C. V. C. S., B. R. C. Costa-Lima, S. P. Suman, M. L. G. Monteiro, F. M. Viana, A. P. A. A. Salim, M. N. Nair, T. J. P. Silva, and C. A. Conte-Junior. 2016. Color attributes and oxidative stability of longissimus lumborum and psoas major muscles from Nellore bulls. *Meat Sci.* 121:19–26. <https://doi.org/10.1016/j.meatsci.2016.05.015>.
- Canto, A. C. V. C. S., S. P. Suman, M. N. Nair, S. Li, G. Rentfrow, C. M. Beach, T. J. P. Silva, T. L. Wheeler, S. D. Shackelford, A. Grayson, R. O. McKeith, and D. A. King. 2015. Differential abundance of sarcoplasmic proteome explains animal effect on beef Longissimus lumborum color stability. *Meat Sci.* 102:90–98. <https://doi.org/10.1016/j.meatsci.2014.11.011>.
- Cheng, S., M. Luo, C. Ding, C. Peng, Z. Lv, R. Tong, H. Xiao, H. Xie, L. Zhou, J. Wu, and S. Zheng. 2016. Downregulation of peptidylprolyl isomerase A promotes cell death and enhances doxorubicin-induced apoptosis in hepatocellular carcinoma. *Gene*. 592:236–244. <https://doi.org/10.1016/j.gene.2016.07.020>.
- Churchman, M. L., J. Low, C. Qu, E. M. Paietta, L. H. Kasper, Y. Chang, D. Payne-Turner, M. J. Althoff, G. Song, S. C. Chen, J. Ma, M. Rusch, D. McGoldrick, M. Edmonson, P. Gupta, Y. D. Wang, W. Caufield, B. Freeman, L. Li, J. C. Panetta, S. Baker, Y.-L. Yang, K. G. Roberts, K. McCastlain, I. Iacobucci, J. L. Peters, V. E. Centonze, F. Notta, S. M. Dobson, S. Zandi, J. E. Dick, L. Janke, J. Peng, K. Kodali, V. Pagala, J. Min, A. Mayasundari, R. T. Williams, C. L. Willman, J. Rowe, S. Luger, R. A. Dickins, R. K. Guy, T. Chen, and C. G. Mullighan. 2015. Efficacy of retinoids in IKZF1-mutated BCR-ABL1 acute lymphoblastic leukemia. *Cancer Cell*. 28:343–356. <https://doi.org/10.1016/j.ccell.2015.07.016>.
- Coleman S. R., M. L. Smith, V. Spicer, Y. Lao, N. Mookherjee, and R. E. W. Hancock. 2020. Overexpression of the small RNA PA0805.1 in *Pseudomonas aeruginosa* modulates the expression of a large set of genes and proteins, resulting in altered motility, cytotoxicity, and tobramycin resistance. *mSystems*. 5:e00204–20. <https://doi.org/10.1128/mSystems.00204-20>.
- Doyle, V., S. Virji, and M. Crompton. 1999. Evidence that cyclophilin-A protects cells against oxidative stress. *Biochem. J.* 341:127–132. <https://doi.org/10.1042/bj3410127>.
- Dröse, S., and U. Brandt. 2008. The mechanism of mitochondrial superoxide production by the cytochrome bc1 Complex. *J. Biol. Chem.* 283:21649–21654. <https://doi.org/10.1074/jbc.M803236200>.
- Dzeja, P., and A. Terzic. 2009. Adenylate kinase and AMP signaling networks: Metabolic monitoring, signal communication and body energy sensing. *Int. J. Mol. Sci.* 10:1729–1772. <https://doi.org/10.3390/ijms10041729>.
- Echevarne, C., M. Renerre, and R. Labas. 1990. Metmyoglobin reductase activity in bovine muscles. *Meat Sci.* 27:161–172. [https://doi.org/10.1016/0309-1740\(90\)90063-C](https://doi.org/10.1016/0309-1740(90)90063-C).
- El Midaoui, A., J. L. Chiasson, G. Tancrede, and A. Nadeau. 2005. Physical training reverses defect in 3-ketoacid CoA-transferase activity in skeletal muscle of diabetic rats. *Am. J. Physiol. -Endoc. M.* 288:748–752. <https://doi.org/10.1152/ajpendo.00515.2004>.
- Fabregat, A., K. Sidiropoulos, G. Viteri, P. Marin-Garcia, P. Ping, L. Stein, P. D'Eustachio, and H. Hermjakob. 2018. Reactome diagram viewer: Data structures and strategies to boost performance. *Bioinformatics*. 34:1208–1214. <https://doi.org/10.1093/bioinformatics/btx752>.
- Galbraith, J. K., J. L. Aalhus, M. Juárez, M. E. R. Dugan, I. L. Larsen, N. Aldai, L. A. Goonewardene, and E. K. Okine. 2016. Meat colour stability and fatty acid profile in commercial bison and beef. *Journal of Food Research*. 5:92. <https://doi.org/10.5539/jfr.v5n3p92>.
- Galbraith, J. K., G. Hauer, L. Helbig, Z. Wang, M. J. Marchello, and L. A. Goonewardene. 2006. Nutrient profiles in retail cuts of bison meat. *Meat Sci.* 74:648–654. <https://doi.org/10.1016/j.meatsci.2006.05.015>.

- Genova, M. L., B. Ventura, G. Giuliano, C. Bovina, G. Formigini, G. Parenti Castelli, and G. Lenaz. 2001. The site of production of superoxide radical in mitochondrial Complex I is not a bound ubiquinone but presumably iron-sulfur cluster N2. *FEBS Lett.* 505:364–368. [https://doi.org/10.1016/S0014-5793\(01\)02850-2](https://doi.org/10.1016/S0014-5793(01)02850-2).
- Hasan, M. M., V. Sood, C. Erkinbaev, J. Paliwal, S. Suman, and A. Rodas-Gonzalez. 2021. Principal component analysis of lipid and protein oxidation products and their impact on color stability in bison longissimus lumborum and psoas major muscles. *Meat Sci.* 178:108523. <https://doi.org/10.1016/j.meatsci.2021.108523>.
- Heberle, H., V. G. Meirelles, F. R. da Silva, G. P. Telles, and R. Minghim. 2015. InteractiVenn: A web-based tool for the analysis of sets through Venn diagrams. *BMC Bioinformatics.* 16:1–7. <https://doi.org/10.1186/s12859-015-0611-3>.
- Hunt, M. C., and H. B. Hedrick. 1977. Fiber types and related properties materials & methods. *J. Food Sci.* 42:513–517.
- Hwang, Y. H., G. D. Kim, J. Y. Jeong, S. J. Hur, and S. T. Joo. 2010. The relationship between muscle fiber characteristics and meat quality traits of highly marbled Hanwoo (Korean native cattle) steers. *Meat Sci.* 86:456–461. <https://doi.org/10.1016/j.meatsci.2010.05.034>.
- Joseph, P., S. P. Suman, S. Li, C. M. Beach, L. Steinke, and M. Fontaine. 2010. Characterization of bison (*Bison bison*) myoglobin. *Meat Sci.* 84:71–78. <https://doi.org/10.1016/j.meatsci.2009.08.014>.
- Joseph, P., S. P. Suman, G. Rentfrow, S. Li, and C. M. Beach. 2012. Proteomics of muscle-specific beef color stability. *J. Agr. Food Chem.* 60:3196–3203. <https://doi.org/10.1021/jf204188v>.
- Ke, Y., R. M. Mitacek, A. Abraham, G. G. Mafi, D. L. VanOverbeke, U. Desilva, and R. Ramanathan. 2017. Effects of muscle-specific oxidative stress on cytochrome c release and oxidation-reduction potential properties. *J. Agr. Food Chem.* 65:7749–7755. <https://doi.org/10.1021/acs.jafc.7b01735>.
- Kim, Y. H., M. C. Hunt, R. A. Mancini, M. Seyfert, T. M. Loughin, D. H. Kropf, and J. S. Smith. 2006. Mechanism for lactate-color stabilization in injection-enhanced beef. *J. Agr. Food Chem.* 54:7856–7862. <https://doi.org/10.1021/jf061225h>.
- Kirchofer, K. S., C. R. Calkins, and B. L. Gwartney. 2002. Fiber-type composition of muscles of the beef chuck and round. *J. Anim. Sci.* 80:2872–2878. <https://doi.org/10.2527/2002.80112872x>.
- Koch, R. M., H. G. Jung, J. D. Crouse, V. H. Varel, and L. V. Cundiff. 1995. Growth, digestive capability, carcass, and meat characteristics of *Bison bison*, *Bos taurus*, and *Bos x Bison*. *J. Anim. Sci.* 73:1271–1281. <https://doi.org/10.2527/1995.7351271x>.
- Kushnareva, Y., A. N. Murphy, and A. Andreyev. 2002. Complex I-mediated reactive oxygen species generation: Modulation by cytochrome c and NAD(P)⁺ oxidation-reduction state. *Biochem. J.* 368:545–553. <https://doi.org/10.1042/BJ20021121>.
- Kyu, J. C., J. P. Yu, J. L. Min, H. K. Jin, J. Ha, W. Choe, and S. K. Sung. 2007. Overexpressed cyclophilin A in cancer cells renders resistance to hypoxia- and cisplatin-induced cell death. *Cancer Res.* 67:3654–3662. <https://doi.org/10.1158/0008-5472.CAN-06-1759>.
- Lee, S. P., Y. S. Hwang, Y. J. Kim, K. S. Kwon, H. J. Kim, K. Kim, and H. Z. Chae. 2001. Cyclophilin A binds to peroxiredoxins and activates its peroxidase activity. *J. Biol. Chem.* 276:29826–29832. <https://doi.org/10.1074/jbc.M101822200>.
- Li, Z., M. Li, X. Li, J. Xin, Y. Wang, Q. W. Shen, and D. Zhang. 2018. Quantitative phosphoproteomic analysis among muscles of different color stability using tandem mass tag labeling. *Food Chem.* 249:8–15. <https://doi.org/10.1016/j.foodchem.2017.12.047>.
- Li, Y., J.-S. Park, J.-H. Deng, and Y. Bai. 2006. Cytochrome c oxidase subunit IV is essential for assembly and respiratory function of the enzyme complex. *J. Bioenerg. Biomembr.* 38:283–291. <https://doi.org/10.1007/s10863-006-9052-z>.
- Liu, R., Q. Fu, S. Lonergan, E. Huff-Lonergan, L. Xing, L. Zhang, Y. Bai, G. Zhou, and W. Zhang. 2018. Identification of S-nitrosylated proteins in postmortem pork muscle using modified biotin switch method coupled with isobaric tags. *Meat Sci.* 145:431–439. <https://doi.org/10.1016/j.meatsci.2018.07.027>.
- Maciel, L., D. F. de Oliveira, G. Monnerat, A. C. Campos de Carvalho, and J. H. M. Nascimento. 2020. Exogenous 10 kDa-heat shock protein preserves mitochondrial function after hypoxia/reoxygenation. *Front. Pharmacol.* 11:545. <https://doi.org/10.3389/fphar.2020.00545>.
- Mancini, R. A., and M. C. Hunt. 2005. Current research in meat color. *Meat Sci.* 71:100–121. <https://doi.org/10.1016/j.meatsci.2005.03.003>.
- Mancini, R. A., K. Belskie, S. P. Suman, and R. Ramanathan. 2018. Muscle-specific mitochondrial functionality and its influence on fresh beef color stability. *J. Food Sci.* 83:2077–2082. <https://doi.org/10.1111/1750-3841.14219>.
- Marchello, M. J., and J. A. Driskell. 2001. Nutrient composition of grass- and grain-finished bison. *Great Plains Research.* 11:65–82. <http://www.jstor.org/stable/23775641>.
- Matarneh, S. K., E. M. England, T. L. Scheffler, and D. E. Gerrard. 2017. Chapter 5: The conversion of muscle to meat. In: F. Toldra, editor, *Lawrie's meat science*. 8th edition. Elsevier Ltd., Amsterdam. p. 159–185.
- McKenna, D. R., P. D. Mies, B. E. Baird, K. D. Pfeiffer, J. W. Ellebracht, and J. W. Savell. 2005. Biochemical and physical factors affecting discoloration characteristics of 19 bovine muscles. *Meat Sci.* 70:665–682. <https://doi.org/10.1016/j.meatsci.2005.02.016>.
- Mertz, J., H. Tan, V. Pagala, B. Bai, P. C. Chen, Y. Li, J. H. Cho, T. Shaw, X. Wang, and J. Peng. 2015. Sequential elution interactome analysis of the mind bomb 1 ubiquitin ligase reveals a novel role in dendritic spine outgrowth. *Mol Cell. Proteomics.* 14:1898–1910. <https://doi.org/10.1074/mcp.M114.045898>.
- Misra, H. P., and I. Fridovich. 1972. The generation of superoxide radical during the autoxidation of hemoglobin. *J. Biol. Chem.* 247:6960–6962. [https://doi.org/10.1016/s0021-9258\(19\)44679-6](https://doi.org/10.1016/s0021-9258(19)44679-6).
- Moxness, M. S., L. S. Brunauer, and W. H. Huestis. 1996. Hemoglobin oxidation products extract phospholipids from the membrane of human erythrocytes. *Biochemistry.* 35:7181–7187. <https://doi.org/10.1021/bi952167o>.
- Nair, M. N., S. Li, C. M. Beach, G. Rentfrow, and S. P. Suman. 2018. Changes in the sarcoplasmic proteome of beef muscles with differential color stability during postmortem aging.

- Meat Muscle Biol. 2:1. <https://doi.org/10.22175/mmb2017.07.0037>.
- Narváez-Bravo, C., A. Rodas-González, C. Ding, O. López-Campos, J. Galbraith, I. L. Larsen, J. Ye, D. Siegel, and J. L. Aalhus. 2017. Effects of novel nitrite packaging film on the bacterial growth of bison strip-loin steaks. *J. Food Process. Pres.* 41:1–7. <https://doi.org/10.1111/jfpp.13311>.
- O’Keefe, M., and D. E. Hood. 1982. Biochemical factors influencing metmyoglobin formation on beef from muscles of differing colour stability. *Meat Sci.* 7:209–228. [https://doi.org/10.1016/0309-1740\(82\)90087-0](https://doi.org/10.1016/0309-1740(82)90087-0).
- Oakley, A. 2011. Glutathione transferases: A structural perspective. *Drug Metab. Rev.* 43:138–151. <https://doi.org/10.3109/03602532.2011.558093>.
- Obchoei, S., S. Wongkhan, C. Wongkham, M. Li, Q. Yao, and C. Chen. 2009. Cyclophilin A: Potential functions and therapeutic target for human cancer. *Med. Sci. Monitor.* 15:RA221–232.
- Olsson, M. G., M. Centlow, S. Rutardóttir, I. Stenfors, J. Larsson, B. Hosseini-Maaf, M. L. Olsson, S. R. Hansson, and B. Åkerström. 2010. Increased levels of cell-free hemoglobin, oxidation markers, and the antioxidative heme scavenger α 1-microglobulin in preeclampsia. *Free Radical Bio. Med.* 48:284–291. <https://doi.org/10.1016/j.freeradbiomed.2009.10.052>.
- Panayiotou, C., N. Solaroli, and A. Karlsson. 2014. The many isoforms of human adenylate kinases. *Int. J. Biochem. Cell. B.* 49:75–83. <https://doi.org/https://doi.org/10.1016/j.biocel.2014.01.014>.
- Pietrasik, Z., J. S. Dhanda, P. J. Shand, and R. B. Pegg. 2006. Influence of injection, packaging, and storage conditions on the quality of beef and bison steaks. *J. Food Sci.* 71:S110–S118. <https://doi.org/10.1111/j.1365-2621.2006.tb08913.x>.
- Qi, F., R. K. Pradhan, R. K. Dash, and D. A. Beard. 2011. Detailed kinetics and regulation of mammalian 2-oxoglutarate dehydrogenase. *BMC Biochem.* 12(1). <https://doi.org/10.1186/1471-2091-12-53>.
- Quinlan, C. L., A. L. Orr, I. V. Perevoshchikova, J. R. Treberg, B. A. Ackrell, and M. D. Brand. 2012. Mitochondrial complex II can generate reactive oxygen species at high rates in both the forward and reverse reactions. *J. Biol. Chem.* 287:27255–27264. <https://doi.org/10.1074/jbc.M112.374629>.
- Ramanathan, R., and R. A. Mancini. 2018. Role of mitochondria in beef color: A review. *Meat Muscle Biol.* 2(1). <https://doi.org/10.22175/mmb2018.05.0013>.
- Ramanathan, R., M. C. Hunt, R. A. Mancini, M. N. Nair, M. L. Denzer, S. P. Suman, and G. G. Mafi. 2020a. Recent updates in meat color research: Integrating traditional and high-throughput approaches. *Meat Muscle Biol.* 4(2). <https://doi.org/10.22175/mmb.9598>.
- Ramanathan, R., M. K. R. Konda, R. A. Mancini, and C. Faustman. 2009. Species-specific effects of sarcoplasmic extracts on lipid oxidation *in vitro*. *J. Food Sci.* 74:C73–C77. <https://doi.org/10.1111/j.1750-3841.2008.01021.x>.
- Ramanathan, R., M. N. Nair, M. C. Hunt, and S. P. Suman. 2019. Mitochondrial functionality and beef colour: A review of recent research. *S. Afr. J. Anim. Sci.* 49:9–19. <https://doi.org/10.4314/sajas.v49i1.2>.
- Ramanathan, R., M. N. Nair, Y. Wang, S. Li, C. M. Beach, R. A. Mancini, K. Belskie, and S. P. Suman. 2021. Differential abundance of mitochondrial proteome influences the color stability of beef longissimus lumborum and psoas major muscles. *Meat Muscle Biol.* 5:1–16. <https://doi.org/10.22175/mmb.11705>.
- Ramanathan, R., S. P. Suman, and C. Faustman. 2020b. Biomolecular interactions governing fresh meat color in post-mortem skeletal muscle: A review. *J. Agr. Food Chem.* 68:12779–12787. <https://doi.org/10.1021/acs.jafc.9b08098>.
- Rule, D. C., K. S. Broughton, S. M. Shellito, and G. Maiorano. 2002. Comparison of muscle fatty acid profiles and cholesterol concentrations of bison, beef cattle, elk, and chicken. *J. Anim. Sci.* 80:1202–1211. <https://doi.org/10.2527/2002.8051202x>.
- Sadrzadeh, S. M. H., E. Graf, S. S. Panter, P. E. Hallaway, and J. W. Eaton. 1984. Hemoglobin: A biologic Fenton reagent. *J. Biol. Chem.* 259:14354–14356. [https://doi.org/10.1016/s0021-9258\(17\)42604-4](https://doi.org/10.1016/s0021-9258(17)42604-4).
- Salim, A. P. A. A., Wang, Y., Li, S., Conte-Junior, C. A., Chen, J., Zhu, H., Rentfrow, G., and Suman, S. P. 2020. Sarcoplasmic proteome profile and internal color of beef longissimus lumborum steaks cooked to different endpoint temperatures. *Meat Muscle Biol.* 4(1). <https://doi.org/10.22175/mmb.9470>.
- Smith, G., K. Belk, J. Sofos, J. Tatum, and S. N. Williams. 2000. Economic implications of improved color stability in beef. In: *Antioxidants in muscle foods: Nutritional strategies to improve quality*. John Wiley and Sons, New York. p. 397–426.
- Suman, S. P., C. Faustman, S. L. Stamer, and D. C. Liebler. 2006. Redox instability induced by 4-hydroxy-2-nonenal in porcine and bovine myoglobins at pH 5.6 and 4°C. *J. Agr. Food Chem.* 54:3402–3408. <https://doi.org/10.1021/jf052811y>.
- Suman, S. P., M. C. Hunt, M. N. Nair, and G. Rentfrow. 2014. Improving beef color stability: Practical strategies and underlying mechanisms. *Meat Sci.* 98:490–504. <https://doi.org/10.1016/j.meatsci.2014.06.032>.
- Suzuki, J., Z. G. Jin, D. F. Meoli, T. Matoba, and B. C. Berk. 2006. Cyclophilin A is secreted by a vesicular pathway in vascular smooth muscle cells. *Circ. Res.* 98:811–817. <https://doi.org/10.1161/01.RES.0000216405.85080.a6>.
- Szklarczyk, D., A. L. Gable, D. Lyon, A. Junge, S. Wyder, J. Huerta-Cepas, M. Simonovic, N. T. Doncheva, J. H. Morris, P. Bork, L. J. Jensen, and C. Von Mering. 2019. STRING v11: Protein-protein association networks with increased coverage, supporting functional discovery in genome-wide experimental datasets. *Nucleic Acids Res.* 47:D607–D613. <https://doi.org/10.1093/nar/gky1131>.
- Turrens, J. F., and A. Boveris. 1980. Generation of superoxide anion by the NADH dehydrogenase of bovine heart mitochondria. *Biochem. J.* 191:421–427. <https://doi.org/10.1042/bj1910421>.
- Vakifahmetoglu-Norberg, H., A. T. Ouchida, and E. Norberg. 2017. The role of mitochondria in metabolism and cell death. *Biochem. Bioph. Res. Co.* 482:426–431. <https://doi.org/10.1016/j.bbrc.2016.11.088>.
- Wang, X., A. K. Pandey, M. K. Mulligan, E. G. Williams, K. Mozhui, Z. Li, V. Jovaisaite, L. D. Quarles, Z. Xiao, J. Huang, J. A. Capra, Z. Chen, W. L. Taylor, L. Bastarache, X. Niu, K. S. Pollard, D. C. Ciobanu, A. O. Reznik, A. V.

- Tishkov, I. B. Zhulin, J. Peng, S. F. Nelson, J. C. Denny, J. Auwerx, L. Lu, and R. W. Williams. 2016. Joint mouse-human phenome-wide association to test gene function and disease risk. *Nat. Commun.* 7. <https://doi.org/10.1038/ncomms10464>.
- Xiong, Y. L. 2018. Chapter 5: Muscle proteins. In: R. Y. Yada, editor, *Proteins in food processing*. 2nd edition. Elsevier Ltd., Amsterdam. p. 127–148.
- Yan, L. J., and R. S. Sohal. 1998. Mitochondrial adenine nucleotide translocase is modified oxidatively during aging. *P. Natl. Acad. Sci. USA.* 95:12896–12901. <https://doi.org/10.1073/pnas.95.22.12896>.
- Yu, Q., X. Tian, L. Shao, L. Xu, R. Dai, and X. Li. 2018. Label-free proteomic strategy to compare the proteome differences between longissimus lumborum and psoas major muscles during early postmortem periods. *Food Chem.* 269:427–435. <https://doi.org/10.1016/j.foodchem.2018.07.040>.
- Yu, Q., W. Wu, X. Tian, M. Hou, R. Dai, and X. Li. 2017a. Unraveling proteome changes of Holstein beef *M. semitendinosus* and its relationship to meat discoloration during post-mortem storage analyzed by label-free mass spectrometry. *J. Proteomics.* 154:85–93. <https://doi.org/10.1016/j.jprot.2016.12.012>.
- Yu, Q., W. Wu, X. Tian, F. Jia, L. Xu, R. Dai, and X. Li. 2017b. Comparative proteomics to reveal muscle-specific beef color stability of Holstein cattle during post-mortem storage. *Food Chem.* 229:769–778. <https://doi.org/10.1016/j.foodchem.2017.03.004>.
- Zhai, C., B. A. Djimsa, J. E. Prenni, D. R. Woerner, K. E. Belk, and M. N. Nair. 2020. Tandem mass tag labeling to characterize muscle-specific proteome changes in beef during early post-mortem period. *J. Proteomics.* 222:103794. <https://doi.org/10.1016/j.jprot.2020.103794>.
- Zhai, C., S. P. Suman, M. N. Nair, S. Li, X. Luo, C. M. Beach, B. N. Harsh, D. D. Boler, A. C. Dilger, and D. W. Shike. 2019. Supranutritional supplementation of vitamin E influences mitochondrial proteome profile of post-mortem longissimus lumborum from feedlot heifers. *S. Afr. J. Anim. Sci.* 48:1140–1147. <https://doi.org/10.4314/sajas.v48i6.18>.
- Zhao, D., L. Chen, C. Qin, H. Zhang, P. Wu, and F. Zhang. 2010. A delta-class glutathione transferase from the Chinese mitten crab *Eriocheir sinensis*: cDNA cloning, characterization and mRNA expression. *Fish Shellfish Immun.* 29:698–703. <https://doi.org/10.1016/j.fsi.2010.06.002>.